Supporting Information

Xanthene-Based Near-Infrared Chromophores for High-Contrast Fluorescence and Photoacoustic Imaging of Dipeptidyl Peptidase 4

Pei Lu, Si-Min Dai, Huihui Zhou, Fenglin Wang,* Wan-Rong Dong* and Jian-Hui Jiang

State Key Laboratory of Chemo/Bio-Sensing and Chemometric, College of Chemistry and Chemical Engineering, Hunan University Changsha, 410082 (P. R. China)

E-mail: fengliw@hnu.edu.cn; wanrongdong@hnu.edu.cn

Table of contents

1. Experimental Procedures

1.1 Reagents and instruments

Dipeptidyl peptidase IV (DPPIV), leucine aminopeptidase (LAP), dipeptidyl peptidases VIII (DPP VIII) and prolidase (PAP) were obtained from Sigma-Aldrich (MO, USA). Recombinant human aminopeptidase N (APN), fibroblast activation protein (FAP) and nitroreductase (NTR) were obtained from R&D Systems (MN, USA). NAD(P)H quinone dehydrogenase 1 (NQO1), γ-glutamate transpeptidase (γ-GGT) and carboxylesterases (CE) were purchased from Biolegend (CA, USA). Phenylmethanesulfonyl fluoride (PMSF) and RIPA-lysis buffer (middle) were purchased from Beyotime (Shanghai, China). DPPIV/CD26 rabbit antibody was purchased from Cell Signaling Technology (MA, USA). β-Actin rabbit monoclonal antibody, horse radish peroxidase (HRP)-conjugated goat anti-rabbit IgG and Alexa Fluor 488-conjugated goat anti-rabbit IgG were obtained by Sangon Biotech (Shanghai, China). Hydrogen peroxide (H_2O_2), cysteine (Cys) and glutathione (GSH) were obtained from J&K Chemicals (Beijing, China). Cell counting Kit-8 (CCK-8) was obtained from Topscience (Shanghai, China). HepG2 cells (human hepatoma cell line) and PC3 (prostate cancer cell line) were obtained from Cell Bank of Type Culture Collection of Chinese Academy of Sciences (Beijing, China). HeLa cells (human cervical carcinoma cell line), MCF-7 cells (human breast adenocarcinoma cell line), HEK293T cells (human embryonic kidney cell line) and A549 cells (non-small cell lung cancer cell line) were purchased from the cell bank of central laboratory at Xiangya Hospital (Changsha, China). Dulbecco's modified Eagle's medium (DMEM), penicillin, streptomycin and 100% heat-inactivated fetal bovine serum were obtained from Thermo Scientific HyClone (MA, USA). Female BALB/c nude mice (4 weeks old, weighing 11-15 g) were provided by Hunan Shrek Jingda Experimental Animal Cooperation (Hunan, China). All other reagents were commercially purchased and used without purification unless otherwise indicated. Ultrapure water was obtained through a Millipore Milli-Q water purification system (Billerica, MA, USA) and had an electric resistance >18.25 MΩ.

Thin-layer chromatography (TLC) was performed on silica gel aluminum sheets with an F-254 indicator. Column chromatography was conducted using 200-300 mesh SiO_2 (Qingdao Ocean Chemical Products). Mass spectroscopy (MS) analysis was performed on an LCQ advantage ion trap mass spectrometry (Thermo Fisher Scientific, Bremen, Germany). ^1H NMR and ^{13}C NMR spectra were recorded on a Bruker Avance-III 400 instrument (Bruker) using tetramethylsilane (TMS) as an internal standard. Mass spectrometric analysis was performed using a Waters Xevo TQ-S triple quadrupole tandem mass spectrometer (Milford, MA, USA) equipped with an electrospray ionization (ESI) source in positive ion mode. pH was determined using a Mettler-Toledo FE20 pH meter. HRMS analysis was performed on ultra-high resolution liquid chromatography mass spectrometry (Thermo Fisher Scientific, Bremen, Germany). Fluorescence spectra were recorded on an FS5 spectrofluorometer (Edinburgh Instruments, United Kingdom). UV-vis absorbance spectra were recorded on a Shimadzu UV-2450 spectrophotometer with an interval of 1 nm. Fluorescence spectra were recorded on an FS5 spectrofluorometer (Edinburgh, UK). Confocal fluorescence imaging was performed on a Nikon A1+ confocal microscope (Japan) with 60× objective lens. In vivo fluorescence imaging was performed on an IVIS Lumina XR small animal imaging system (Caliper, Switzerland). All the photoacoustic imaging experiments were performed on a multispectral optoacoustic tomographic (MSOT) imaging system (inVision256-TF, iThera Medical GmbH).

1.2 In vitro Assays

Absorption, fluorescence and PA measurements. To study the responses of RhoMQ-DPPIV/RhoMA-DPPIV towards DPPIV, RhoMQ-DPPIV/RhoMA-DPPIV (5 μM) was incubated with DPPIV (2.0 μg/mL) in pH 7.4 buffer at 37 °C for 1 h. To determine the ability of RhoMQ-DPPIV/RhoMA-DPPIV to quantitatively detecting DPPIV activity, RhoMQ-DPPIV/RhoMA-DPPIV (5 μM) was incubated with varying concentrations of DPPIV. The limit of

detection was calculated using the following equation:

$$\text{Detection limit} = 3\sigma/k$$

Where σ is the standard deviation of the blank measurements, k is the slope between the fluorescence/PA intensity at 775 nm/690 nm versus various DPPIV concentrations (0-2.0 μg/mL) in the linear region.

For selectivity studies, solutions of various testing substances including H_2O_2 (100 μM), Cys (100 μM), GSH (5 mM), serum (20%), Trypsine (0.25%), BSA (2.0 μg/mL), NAD(P)H quinone dehydrogenase 1 (NQO1, 2.0 μg/mL), nitroreductase (NTR, 2.0 μg/mL), APN (2.0 μg/mL), gamma-glutamyl transferase (γ-GGT, 2.0 μg/mL), carboxylesterases (CE, 2.0 μg/mL) carboxylesterases (CE, 2.0 μg/mL), leucine aminopeptidase (LAP, 2.0 μg/mL), prolidase (PAP, 2.0 μg/mL), dipeptidyl peptidases VIII (DPP VIII, 2.0 μg/mL), fibroblast activation protein (FAP, 2.0 μg/mL) and DPPIV (2.0 μg/mL) were incubated with RhoMQ-DPPIV/RhoMA-DPPIV (5 μM) at 37 °C for 1 h.

For DPPIV inhibition, RhoMQ-DPPIV/RhoMA-DPPIV (5 μM) was treated with sitagliptin (50 μM) and DPPIV (2.0 μg/mL) in pH 7.4 buffer at 37 °C for 1 h. Fluorescence spectra were recorded in the range from 600 nm to 880 nm with an excitation wavelength of 580 nm. Photoacoustic experiments were performed on a multispectral optoacoustic tomographic (MSOT) imaging system.

For cell lysate assays, HepG2 cells were lysed in lysis buffer and the lysates were collected. RhoMQ-DPPIV/RhoMA-DPPIV (5 μM) was incubated with cell lysate in pH 7.4 buffer at 37 °C for 1 h. Fluorescence spectra and photoacoustic data were collected.

Photostability studies. For photostability studies, RhoMQ, RhoI, RhoBTA and cyanine 5 (Cy5) in PBS (10 mM, pH = 7.4) containing 1% DMSO was irradiated with a xenon lamp (100 W) and maximum fluorescence intensities were recorded at different time points for 2 h.

Calculations of Fluorescence Quantum Yield of RhoMQ, RhoI, RhoBTA. The fluorescence quantum yields of RhoMQ, RhoI, RhoBTA were determined according to the following equation using Cy5 (Φ_f = 0.27 in PBS) as a reference according to the literature[1].

$$\Phi_x = \Phi_s \times (I_x/I_s) \times (A_s/A_x) \times (n_x/n_s)^2$$

Φ denotes the quantum yield; I denotes the area under the emission spectra; A denotes the absorbance at the excitation wavelength; n denotes the refractive index of the solvent. S and X represent the reference standard and unknown sample, respectively.

HPLC and HR-MS-ESI analysis. Probe RhoMQ-DPPIV/RhoMA-DPPIV (20 μM) was incubated with DPPIV (8.0 μg/mL) in PBS (10 mM, pH 7.4) for 1 h at 37 °C. The reaction was quenched by 250 μL of acetonitrile, vortexed and centrifuged at 10000 rpm for 15 min. HPLC and HR-MS-ESI analysis was performed.

Lineweaver-Burk analysis. Lineweaver-Burk analysis for DPPIV-catalyzed decaging of RhoMQ-DPPIV was investigated using FS5 assays. DPPIV (2.0 μg/mL) was incubated with different concentrations of RhoMQ-DPPIV (1 μM, 2 μM, 5 μM, 8 μM and 10 μM) in PBS (10 mM, pH 7.4) at 37 °C for 1 h and fluorescence spectra were then recorded on a FS5 spectrofluorometer. Data was analyzed with the Lineweaver-Burk curve. Kinetic parameters were calculated according to the Michaelis Menten equation: $V = V_{max}[S] / (K_m + [S])$ or $V = K_{cat}[E]_t[S] / (K_m + [S])$, where V is the reaction rate, [S] is the concentration of RhoMQ-DPPIV and $[E]_t$ is the concentration of DPPIV.

1.3 Cellular Studies

Cell culture. Cells of HepG2, PC3, HEK293T, HeLa, MCF-7 and A549 were cultured in DMEM supplemented with 10% fetal bovine serum, 100 U/mL penicillin and 100 g/mL streptomycin at 37 °C in a humidified atmosphere

containing 5% CO_2. The cells were plated on 35 mm sterilized dishes with 14 mm wells and grown to a confluency of 50-70%.

Cytotoxicity assay. Cells were seeded in 96-well plates at a density of 1×10^4 cells per well and cultured for 24 h. The cells were incubated with different concentrations of RhoMQ-DPPIV/RhoMA-DPPIV (0 μM - 40 μM) for 24 h before addition of CCK-8 solution (10 μL). The cells were incubated at 37 °C for 2 h and optical density (OD) values at 450 nm were measured with a microplate reader. Cell viability was determined using the following equation:

$$\text{Cell viability (\%)} = (OD_{probe} - OD_{blank})/(OD_{control} - OD_{blank}) \times 100$$

where OD_{probe} are the OD values for cells treated with dROA-QL/dROA-AD (0 μM - 40 μM).

Cell imaging. Confocal fluorescence images were performed according to the following procedure: All cells were incubated with 1 mL fresh culture medium containing probe RhoMQ-DPPIV (5 μM) at 37 °C for 1 h. The cells were washed with cold PBS for three times before imaging. For inhibition study, cells were pretreated with sitagliptin (50 μM) for 1 h before incubation with the probe RhoMQ-DPPIV (5 μM). Fluorescence images were acquired using a Nikon A1+ confocal microscope.

PA images of cells were performed as follows: HepG2 cells were incubated with RhoMA-DPPIV (5 μM) at 37 °C for 1 h. For inhibition study, HepG2 cells were pretreated with sitagliptin (50 μM) for 1 h before incubation with RhoMA-DPPIV (5 μM). After incubation, the cells were washed with PBS for three times. Cells were harvested with 0.25% trypsin and counted with a TC20™ automated cell counter (BIO-RAD, USA). The cell suspension was collected with a microtube (200 μL) by centrifugation. Tubes with the cell pellets were inserted into the tube holder and imaged with the MSOT imaging system.

Flow cytometry assays. All the cells were cultured in 6-well plates at a density of 2×10^5 cells/well for 24 h and then incubated with probe RhoMQ-DPPIV (5 μM) at 37 °C for 1 h. The cells were washed twice with PBS (pH = 7.4), treated with 0.25% trypsin and centrifuged at 1500 rpm for 3 min at room temperature. The cell pellet was washed and suspended in PBS for flow cytometry analysis on a FACSVerseTM flow cytometer.

Western blotting analysis. Western blotting assay for DPP4 was performed according to the manufacturer's protocols with slight modifications. HepG2, A549, MCF-7, HeLa, PC3, HEK293T cells were lysed in lysis buffer and total proteins were extracted. The extracted proteins were separated by SDS-PAGE and transferred to polyvinylidene difluoride (PVDF) membranes. The membranes were blocked with I-Block reagent (0.2%) containing bovine saline albumin (5%) and incubated with primary antibodies (1: 1000 dilution) at room temperature overnight. The membranes were washed with 1× TBST buffer and incubated with HRP-conjugated secondary antibodies (1: 3000 dilution) for 2 h. A chemiluminescence system (Thermo Fisher) was used to visualize the immunoreactive bands. For control, β-actin was analyzed using the same protocol using the corresponding primary antibody.

1.4 Vivo Studies

Tumor Mouse Model. All mice experiments were approved by the Hunan Provincial Science & Technology Department and performed in compliance with the guidelines of the Institutional Animal Care and Use Committee of Hunan University (approval number: SYXK2018-0006). Female nude mice (4-5 weeks of age) were obtained from Hunan Shrek Jingda Experimental Animal Cooperation (Changsha, China). HepG2 tumor cells (1×10^7 cells in 100 μL 1 × PBS) were subcutaneously inoculated on the left flanks of mice. Tumors were grown to ~100 mm^3 before imaging.

In vivo NIRF imaging and ex vivo fluorescence imaging. To analyze specific activation and the organ

distribution of probe RhoMQ-DPPIV in vivo and ex vivo, the mice bearing HepG2 tumors (~100 mm^3) were randomly divided into three groups (n = 3). Mice from Group 1 and Group 2 were treated with vehicle (PBS, 100 μL) and RhoMQ-DPPIV (100 μM, 100 μL), respectively, by tail-vein injection. For DPPIV activity inhibition, mice from Group 3 were pre-treated with sitagliptin (100 μM in 100 μL PBS), and probe RhoMQ-DPPIV was then administered by tail-vein injection. In vivo NIRF images were acquired before injection (0 h) and at different time points (1 h, 2 h, 3 h, 4 h, 12 h) post injection. For ex vivo NIRF imaging, the mice were euthanized at 3 h post-injection of the probe RhoMQ-DPPIV, tumors and main organs (heart, liver, spleen, lung, kidney) were harvested and imaged. Fluorescence intensities were analyzed with the Living Image 4.0 Software from different ROIs from the tumor regions or organs.

In vivo PA imaging. To analyze specific activation of probe RhoMA-DPPIV in vivo, the mice bearing HepG2 tumors (~100 mm^3) were randomly divided into three groups (n = 3). Mice from Group 1 and Group 2 were treated with vehicle (PBS, 100 μL) and RhoMA-DPPIV (100 μM, 100 μL), respectively, by tail-vein injection. For DPPIV activity inhibition, mice from Group 3 were pre-treated with sitagliptin (100 μM in 100 μL PBS), and probe RhoMA-DPPIV was then administered by tail-vein injection. Mice were anesthetized with isoflurane and placed in a lateral position in an animal scaffold for PA imaging. The entire tumor region was scanned with each wavelength with a step size of 0.3 mm. In vivo MSOT images were acquired before injection (0 min) and at a given time post injection (1 h, 2 h, 3 h, 4 h, 12 h). Linear regression spectral unmixing was introduced to separate signals from the activated probes and those from the photoabsorbers in tissue (e.g. hemoglobin). Mean MSOT intensities were obtained with the ViewMSOT from different regions of interest (ROIs) from the tumor.

Tissue penetration depth evaluation. In vitro fluorescence imaging was performed using the IVIS Lumina XR small animal imaging system (Caliper, Switzerland) under fluorescence modes. RhoMQ-DPPIV/ RhoMA-DPPIV was incubated with DPPIV in pH 7.4 buffer at 37 °C for 1 h. Fluorescence images of RhoMQ in 96-well plate were taken through chicken breast of varying thickness. In vitro PA imaging was performed using a multispectral optoacoustic tomographic (MSOT) imaging system (inVision256-TF, iThera Medical GmbH). PA images of RhoMA in tube were taken through chicken breast of varying thickness.

Haematoxylin and eosin (H&E) staining analysis of major organs. Representative histological features of major organs (heart, liver, spleen, lung, kidney) were excised from HepG2 tumor-bearing mice after treatment. The excised organs and tumor tissues were fixed with 4% formaldehyde solution, embedded in paraffin, and sliced into 5 μm thick. The slices were dewaxed, hydrated, and sequentially stained with haematoxylin and eosin. The slices were rinsed with water and dehydrated for imaging acquisition. Fluorescence images were collected by a fluorescence microscope with a magnification of 100 times.

Immunofluorescence staining analysis. The excised tumors were fixed with 4% formaldehyde, embedded in paraffin and sliced into 5 μm in thickness. For immunofluorescence staining analysis, the sliced tissues were stained with and DAPI, anti-DPPIV antibody, Alexa Fluor 488-conjugated goat anti-rabbit IgG and RhoMQ-DPPIV. Fluorescence images were collected by a fluorescence microscope with a magnification of 20 times.

Blood chemistry assays. BALB/c mice were intravenously injected with PBS (100 μL), RhoMQ-DPPIV (100 μM, 100 μL) and RhoMA-DPPIV (100 μM, 100 μL). Blood was collected for the blood chemistry test one day after the treatments. All the data were expressed as mean ± s.d.

1.5 Synthesis of compounds

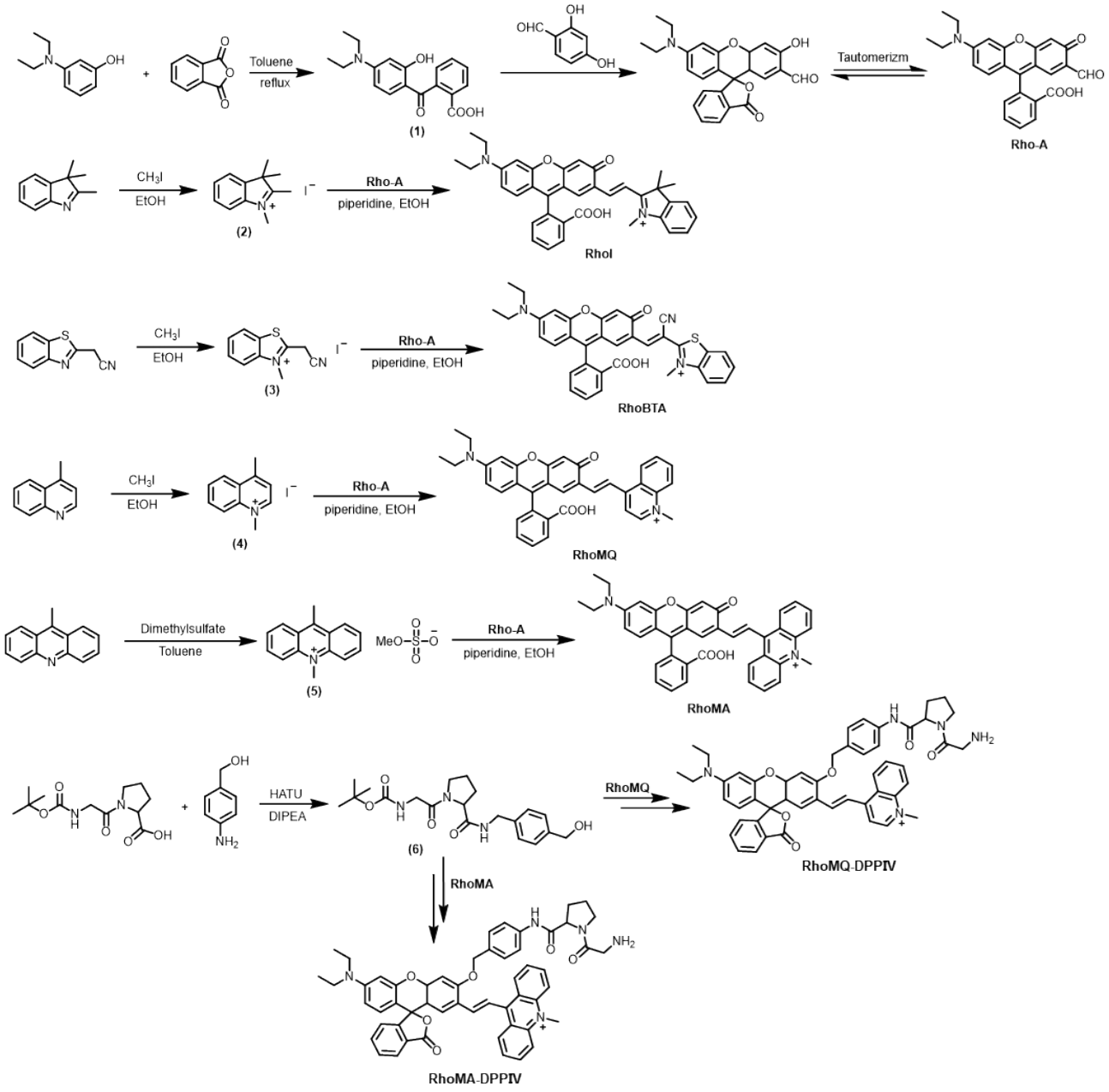

Scheme S1. Synthetic routes for **RhoI, RhoBTA, RhoMQ, RhoMA**, **RhoMQ-DPPIV** and **RhoMA-DPPIV**.

Synthesis of compound 1. A mixture of 3-diethylaminophenol (1.00 g, 6.05 mmol) and o-phthalic anhydride (1.07g, 7.26 mmol) were refluxed in methylbenzene (15 mL) for 4 h. After reaction, the mixture was cooled to room temperature, filtered and washed with methanol. The compound as a pale pink solid was afforded in a yield of 25%. ^{1}H NMR (400 MHz, 298 K, DMSO-d_6): δ 13.07 (s, 1 H), 12.57 (s, 1 H), 7.95 (d, *J* = 8.0 Hz, 1 H), 7.68 (t, *J*= 7.2 Hz, 1 H), 7.61 (t, *J*= 7.2 Hz, 1 H), 7.39 (d, *J*=7.2 Hz, 1 H), 6.80 (d, *J*=9.2 Hz, 1 H), 6.19 (d, *J*= 8.8 Hz, 1 H), 6.08 (s, 1 H), 3.41-3.37 (m, 4H), 1.09 (t, *J*= 6.8 Hz, 6H). ^{13}C NMR (100 MHz, 298 K, DMSO-d_6): δ 198.75, 167.37, 165.13, 153.95, 140.50, 134.69, 132.45, 130.32, 130.14, 129.84, 128.12, 109.73, 104.44, 96.78, 44.78, 12.93. HR-ESI-MS:

m/z calcd for compound **1** ($C_{18}H_{19}NO_4$, $[M+H]^+$, $[M+Na]^+$), 314.35, 336.35; found, 314.13, 336.08.

Synthesis of compound Rho-A. A mixture of compound **1** (300mg, 0.96 mmol) and 2,4-dihydroxybenzaldehyde (132 mg, 0.96 mmol) in methanesulfonic acid (5 mL) were stirred at 90 °C, and monitored by TLC. After reaction, the solution was cooled down to room temperature and poured into ice-cold water (100 mL). The pH was adjusted to 7 with ammonium hydroxide, and the precipitate was filtered, washed with brine and dried under vacuum. The crude was purified by chromatography on a silica gel column (CH_2Cl_2:CH_3OH = 300:1, v/v) to afford **Rho-A** as a red solid. Yield: 20%. ^{1}H NMR (400 MHz, 298 K, $CDCl_3$): δ 11.18 (s, 1 H), 9.57 (s, 1 H), 8.03 (d, *J* = 7.6 Hz, 1 H), 7.72-7.63 (m, 2 H), 7.22 (d, *J* = 7.6 Hz, 1 H), 7.01 (s, 1 H), 6.79 (s, 1 H), 6.55 (d, *J* = 9.2 Hz, 1 H), 6.47 (s, 1 H), 6.39 (d, *J* = 9.2 Hz, 1 H), 3.38-3.34 (m, 4 H), 1.18 (t, *J* = 6.8 Hz, 6 H). ^{13}C NMR (100 MHz, 298 K, $CDCl_3$): δ 194.70, 169.34, 163.01, 157.93, 152.59, 152.29, 149.83, 135.57, 135.14, 129.91, 128.80, 127.05, 125.16, 123.94, 117.91, 113.37, 108.98, 104.60, 104.47, 97.79, 83.04, 44.54, 12.48. ESI-MS: m/z calcd for compound **Rho-A** ($C_{25}H_{21}NO_5$, $[M+H]^+$), 416.45; found, 416.56.

Synthesis of compound 2. 2,3,3-trimethylindolenine (1.0 g, 6.3 mmol) and iodomethane (4.43 g, 31.4 mmol) were dissolved in 10 mL ethanol and the mixture was refluxed overnight. After reaction, the solution was cooled down to room temperature and filtered to afford compound **2** as a pink solid. Yield: 87%. ^{1}H NMR (400 MHz, 298 K, DMSO-d_6): δ 7.90 (d, *J* = 8.8 Hz, 1 H), 7.83 (d, *J* = 8.8 Hz, 1 H), 7.61 (d, *J* = 3.6 Hz, 2 H), 3.97 (s, 3 H), 2.77 (s, 3 H), 1.53 (s, 6 H). ^{13}C NMR (100 MHz, 298 K, DMSO-d_6): δ 196.46, 142.57, 142.06, 129.78, 129.28, 123.76, 115.59, 54.39, 22.17, 14.60. ESI-MS: m/z calcd for compound 2 ($C_{12}H_{16}N^+$, $[M]^+$), 174.27; found, 174.15.

Synthesis of compound 3. Benzothiazole-2-acetonitrile (1.74 g, 10 mmol) and iodomethane (7.1 g, 50 mmol) were reacted at 80 °C for 12 h. The mixture was cooled down to room temperature and precipitated with anhydrous ether, filtered and washed with ether to give compound **3** as a gray solid. Yield: 83%. ^{1}H NMR (400 MHz, 298 K, DMSO-d_6): δ 7.66 (d, *J* = 8.0 Hz, 1 H), 7.33 (t, *J* = 8.0 Hz, 1 H), 7.25 (d, *J* = 8.4 Hz, 1 H), 7.10 (t, *J* = 7.6 Hz, 1 H), 4.70 (s, 1 H), 3.36 (s, 3 H). ^{13}C NMR (100 MHz, 298 K, DMSO-d_6): δ162.67, 142.64, 127.33, 123.20, 122.84, 122.75, 121.51, 111.05, 54.92, 31.98. ESI-MS: m/z calcd for compound **3** ($C_{10}H_9N_2S^+$, $[M]^+$), 189.26; found, 189.10.

Synthesis of compound 4. 4-Methylquinoline (1.43 g, 10 mmol) and iodomethane (7.1 g, 50 mmol) were dissolved in 10 mL ethanol, the mixture was stirred and refluxed overnight. After reaction, the solution was cooled down to room temperature and filtered to afford compound **4** as a yellow solid. Yield: 85%. ^{1}H NMR (400 MHz, 298 K, DMSO-d_6): δ 9.37 (d, *J* = 6.0 Hz, 1 H), 8.53 (d, *J* = 8.4 Hz, 1 H), 8.48 (d, *J* = 8.4 Hz, 1 H), 8.27 (d, *J* = 7.2 Hz, 1 H), 8.06 (t, *J* = 7.2 Hz, 2 H), 4.58 (s, 3 H), 3.01 (s, 3 H). ^{13}C NMR (100 MHz, 298 K, DMSO-d_6): δ 158.65, 149.44, 138.15, 135.40, 130.12, 128.95, 127.27, 122.93, 120.01, 43.51, 20.10. ESI-MS: m/z calcd for compound **4** ($C_{11}H_{12}N^+$, $[M]^+$), 158.22; found, 158.23.

Synthesis of compound 5. 9-Methylacridine (440mg, 2.3 mmol) was dissolved in toluene (10 ml) and added with dimethyl sulfate (652 μL, 6.9 mmol). The mixture was refluxed for 2 h and cooled to room temperature. The yellow precipitate was isolated by filtration and washed with diethyl ether, followed by diethyl ether/dichloromethane to afford the product as a yellow-green powder. Yield: 78%. ^{1}H NMR (400 MHz, 298 K, DMSO-d_6): δ 8.90 (d, *J* = 8.4 Hz, 2 H), 8.74 (d, *J* = 8.4 Hz, 2 H), 8.42 (t, *J* = 6.8 Hz, 2 H), 8.02 (t, *J* = 6.8 Hz, 2 H), 4.81 (s, 2 H), 4.58 (s, 3 H), 3.51 (s, 3 H). ^{13}C NMR (100 MHz, 298 K, DMSO-d_6): δ 161.28, 140.82, 138.70, 128.65, 127.85, 126.02, 119.72, 53.25, 16.94. ESI-MS: m/z calcd for compound **5** ($C_{15}H_{14}N^+$, $[M]^+$), 208.28; found, 208.26.

Synthesis of compound 6. 4-Aminobenzyl alcohol (1.23 g, 10 mmol), L-1-(N-carboxyglycyl) proline N-tert-butyl ester (2.73 g, 10 mmol), O-(7-azabenzotriazol-1-yl)-N, N, N', N'-tetramethyluronium hexafluorophosphate (HATU, 3.8 g, 10 mmol) and N, N-diisopropylethylamine (DIPEA, 2.59 g, 10 mmol) were dissolved in anhydrous THF (15

mL). The mixture was stirred at 0 °C under nitrogen for 10 min and at room temperature overnight. The solvent was removed under vacuum and the dark crude product was purified by silica gel column chromatography using PE/EA (2:1, v/v) as the eluent to obtain compound **6** as a white yellow solid. Yield: 82%. ^{1}H NMR (400 MHz, 298 K, $CDCl_3$): δ 9.39 (s, 1 H), 7.51 (d, *J* = 8.4 Hz, 2 H), 7.29 (d, *J* = 8.4 Hz, 2 H), 5.41 (s, 1 H), 4.79 (d, *J* = 7.2 Hz, 1 H), 4.56 (s, 2 H), 3.97 (t, *J* = 12.8 Hz, 2 H), 3.62-3.42 (m, 2 H), 2.57 (t, *J* = 6.4 Hz, 1 H), 2.21-1.90 (m, 4 H), 1.47 (s, 9 H). ^{13}C NMR (100 MHz, 298 K, $CDCl_3$): δ 169.67, 168.51, 155.85, 138.24, 133.04, 129.26, 119.89, 80.04, 61.04, 46.58, 46.03, 43.16, 38.66, 31.43, 30.20, 28.33, 26.79, 24.96, 0.01. ESI-MS: m/z calcd for compound **6** ($C_{19}H_{27}N_3O_5$, $[M+Na]^+$), 400.44; found, 400.17.

Synthesis of compound RhoI. **Rho-A** (145 mg, 1 mmol) and compound **2** (174 mg, 1 mmol) were dissolved in EtOH (5 mL) and added with piperidine (50 μL). The mixture was refluxed at 80 ℃, and monitored by TLC. After reaction, the solution was cooled down to room temperature. The solvent was removed under vacuum and the crude product was purified by silica gel column chromatography using CH_2Cl_2/MeOH (5 to 20% of MeOH) as an eluent to obtain compound **RhoI** as a dark bule solid. Yield: 27%. ^{1}H NMR (400 MHz, 298 K, MeOD): δ 8.06 (d, *J* = 7.2 Hz, 1 H), 7.78-7.70 (m, 3 H), 7.22 (t, *J* = 6.0 Hz, 1 H), 7.14 (t, *J* = 7.6 Hz, 1 H), 7.07 (t, *J* = 7.6 Hz, 1 H), 6.82 (t, *J* = 7.2 Hz, 1 H), 6.79 (t, *J* = 3.2 Hz, 1 H), 6.66-6.60 (m, 3 H), 6.57-6.55 (m, 3 H), 4.59 (s, 1 H), 3.48-3.42 (m, 4 H), 1.30 (s, 3 H), 1.18 (t, *J* = 6.8 Hz, 6 H), 1.13 (s, 3 H). ^{13}C NMR (100 MHz, 298 K, MeOD): δ 153.51, 150.98, 134.20, 129.66, 129.05, 128.13, 127.28, 125.27, 124.80, 119.13, 109.72, 106.64, 101.79, 96.98, 44.33, 27.76, 18.88, 11.40. HRMS: m/z calcd for compound **RhoI** ($C_{37}H_{37}N_2O_4^+$, $[M]^+$), 571.70; found, 571.2582.

Synthesis of compound RhoBTA. **RhoBTA**, a brown solid (Yield: 20%), was synthesized and purified similarly as **RhoI** using compound **3** (189 mg, 1 mmol). ^{1}H NMR (400 MHz, 298 K, MeOD): δ 8.05 (d, *J* = 7.6 Hz, 1 H), 7.80-7.70 (m, 2 H), 7.57 (t, *J* = 7.2 Hz, 1 H), 7.51 (d, *J* = 7.6 Hz, 1 H), 7.45 (t, *J* = 7.6 Hz, 1 H), 7.33 (t, *J* = 7.6 Hz, 1 H), 7.27-7.18 (m, 2 H), 7.16-7.07 (m, 2 H), 6.78 (d, *J* = 7.6 Hz, 1 H), 6.68 (s, 1 H), 6.55 (t, *J* = 7.6 Hz, 1 H), 3.41 (s, 3 H), 3.22 (m, 4 H), 1.21 (t, *J* = 7.6 Hz, 6 H). ^{13}C NMR (100 MHz, 298 K, MeOD): δ193.25, 163.29, 150.41, 142.22, 134.92, 133.66, 129.88, 128.64, 126.68, 126.62, 122.35, 121.62, 109.96, 30.43, 11.41, 11.36, 7.82. HRMS: m/z calcd for compound **RhoBTA** ($C_{35}H_{28}N_3O_4S^+$, $[M+H]^+$), 587.69; found, 587.1631.

Synthesis of compound RhoMQ. **RhoMQ**, a dark bule solid (Yield: 31%), was synthesized and purified similarly as **RhoI** using compound **4** (158 mg, 1 mmol). ^{1}H NMR (400 MHz, 298 K, MeOD): δ 8.88 (s, 1 H), 8.53-8.43 (m, 2 H), 8.24-7.90 (m, 5 H), 7.72-7.65 (m, 3 H), 7.33 (d, *J* = 6.8 Hz, 2 H), 7.12 (d, *J* = 8.8 Hz, 1 H), 6.82 (d, *J* = 8.8 Hz, 1 H), 6.72 (s, 1 H), 6.43 (s, 1 H), 4.38 (s, 3 H), 3.57 (m, 4 H), 1.26 (t, *J* = 6.8 Hz, 6 H). ^{13}C NMR (100 MHz, 298 K, MeOD): δ 158.63, 156.66, 154.46, 154.22, 147.05, 140.67, 138.97, 134.91, 131.39, 129.57, 129.32, 129.16, 126.58, 125.68, 118.43, 113.29, 111.96, 117.76, 95.99, 29.36, 21.22, 11.52. HRMS: m/z calcd for compound **RhoMQ** ($C_{36}H_{31}N_2O_4^+$, $[M]^+$), 555.65; found, 555.2272.

Synthesis of compound RhoMA. **RhoMA**, a brown solid (Yield: 22%), was synthesized and purified similarly as **RhoI** using compound **5** (208 mg, 1 mmol). ^{1}H NMR (400 MHz, 298 K, MeOD): δ 8.89 (d, *J* = 7.6 Hz, 1 H), 8.49 (d, *J* = 7.6 Hz, 1 H), 8.41 (d, *J* = 8.4 Hz, 1 H), 8.23 (d, *J* = 7.6 Hz, 1 H), 8.15-8.08 (m, 3 H), 8.00 (d, *J* = 6.4 Hz, 1 H), 7.88 (t, *J* = 7.6 Hz, 1 H), 7.74-7.62 (m, 4 H), 7.52-7.40 (m, 3 H), 7.37-7.35 (m, 2 H), 7.13 (d, *J* = 8.0 Hz, 1 H), 6.82 (d, *J* = 6.4 Hz, 1 H), 6.72 (d, *J* = 7.6 Hz, 1 H), 6.38 (d, *J* = 7.6 Hz, 1 H), 4.37 (s, 3 H), 3.62-3.57 (m, 4 H), 1.24 (t, *J* = 7.6 Hz, 6 H). ^{13}C NMR (100 MHz, 298 K, MeOD): δ158.73, 156.83, 154.39, 147.08, 140.72, 138.96, 134.94, 131.54, 129.46, 129.30, 126.55, 120.16, 118.58, 115.07, 113.38, 112.31, 111.89, 104.81, 95.93, 61.40, 45.12, 44.28, 44.10, 30.56, 29.38, 22.34, 21.69, 11.59. HRMS: m/z calcd for compound **RhoMA** ($C_{40}H_{33}N_2O_4^+$, $[M]^+$), 605.71; found, 605.2427.

Synthesis of compound RhoMQ-DPPIV. Compound **6** (0.4 g, 1 mmol) and *p*-toluenyl chloride (0.23 g, 1.2 mmol)

were dissolved in anhydrous DCM (15 mL), and triethylamine (0.1 mL) was slowly added under nitrogen protection at 0 ℃. The mixture was stirred for 3 h and the solvent was removed under vacuum. The crude product was purified by silica gel column chromatography using DCM as mobile phase to obtain a light yellow solid **6-OTs**. Yield: 77%.

Compound **RhoMQ** (55.5 mg, 0.1 mmol), compound **6-OTs** (53.1 mg, 0.1 mmol), potassium carbonate (63 mg, 0.5 mmol) and sodium iodide (15 mg, 0.1 mmol) were dissolved in DMF (20 mL). After stirring at 80 ℃ for 5 h, the solvent was removed under vacuum, and the crude product was purified by silica gel column chromatography with CH_2Cl_2/MeOH (5-20% MeOH) as the eluent to obtain **Boc-RhoMQ-DPPIV** as a solid. Yield: 43%.

Boc-RhoMQ-DPPIV (50.2 mg, 0.05 mmol) was dissolved in anhydrous DCM (10 mL) and added with trifluoroacetic acid (1 mL) at 0 ℃. The resulting mixture was stirred for 1 h at room temperature. The solvent was removed under reduced pressure, and the crude product was purified by silica gel column chromatography with DCM/MeOH = 20/1 as the eluent to afford compound **RhoMQ-DPPIV**. Yield: 74%. ^{1}H NMR (400 MHz, 298 K, MeOD): δ 8.94 (d, *J* = 5.2 Hz, 1 H), 8.54 (d, *J* = 8.0 Hz, 1 H), 8.31 (d, *J* = 8.8 Hz, 1 H),8.20-8.10 (m, 3 H), 7.96 (t, *J* = 7.2 Hz, 1 H), 7.79 (s, 1 H), 7.73 (d, *J* = 8.0 Hz, 2 H), 7.56-7.53 (m, 2 H), 7.41-7.30 (m, 5 H), 7.03-6.97 (m, 1 H), 6.79-6.71 (m, 2 H), 6.56 (s, 1 H), 5.36 (s, 1 H), 4.57 (s, 2 H), 4.47 (s, 3 H), 3.94 (t, *J* = 7.2 Hz, 2 H), 3.67-3.62 (m, 2 H), 3.60-3.54 (m, 4 H), 2.21 (t, *J* = 6.4 Hz, 1 H), 2.21 (t, *J* = 6.4 Hz, 1 H), 1.83-1.63 (m, 4 H), 1.26 (t, *J* = 6.8 Hz, 6 H). ^{13}C NMR (100 MHz, 298 K, MeOD): δ160.16, 158.24, 157.74, 150.91, 144.41, 138.83, 135.01, 134.25, 133.39, 132.97, 132.70, 131.09, 123.76, 122.34, 118.98, 115.45, 100.03, 67.30, 64.85, 52.42, 50.31, 48.91, 48.18, 47.80. HR MS: m/z calcd for compound **RhoMQ-DPPIV** ($C_{50}H_{48}N_5O_6^+$, $[M]^+$), 814.37; found, 814.6310.

Synthesis of compound RhoMA-DPPIV. Compound **RhoMA-DPPIV** was synthesized similarly as **RhoMQ-DPPIV** using compound **RhoMA** (60.5 mg, 0.1 mmol). Yield: 23%. ^{1}H NMR (400 MHz, 298 K, MeOD): δ 8.81 (d, *J* = 5.2 Hz, 1 H), 8.40-8.36 (m, 3 H), 8.18-8.04 (m, 4 H), 7.93 (d, *J* = 6.4 Hz, 1 H), 7.84 (t, *J* = 6.4 Hz, 1 H), 7.68-7.63 (m, 2 H), 7.57-7.47 (m, 3 H), 7.29-7.21 (m, 4 H), 7.01 (d, *J* = 8.8 Hz, 1 H), 6.74 (d, *J* = 8.8 Hz, 1 H), 6.63 (d, *J* = 6.4 Hz, 1 H), 6.38 (s, 1 H), 5.31 (s, 1 H), 4.51 (s, 2 H), 4.32 (s, 3 H), 3.88 (t, *J* = 7.2 Hz, 2 H), 3.62-3.57 (m, 2 H), 3.53-3.50 (m, 4 H), 2.17 (t, *J* = 6.4 Hz, 1 H), 2.21 (t, *J* = 7.6 Hz, 1 H), 1.77-1.73 (m, 2 H), 1.65-1.55 (m, 2 H),1.21 (t, *J* = 6.8 Hz, 6 H). ^{13}C NMR (100 MHz, 298 K, DMSO-d_6): δ 158.84, 158.61, 149.46, 135.37, 130.08, 129.66, 127.21, 119.95, 119.19, 116.21, 113.94, 58.46, 48.99, 48.09, 47.88, 45.42, 45.09, 44.31, 43.93, 37.97, 31.93, 30.81, 29.85, 29.52, 29.48, 29.43, 29.27, 29.15, 29.02, 28.30, 26.99, 22.55, 22.15, 14.38, 12.75. HRMS: m/z calcd for compound **RhoMA-DPPIV** ($C_{54}H_{50}N_5O_6^+$, $[M+H]^+$), 865.38; found, 865.2699.

2. Supplementary figures

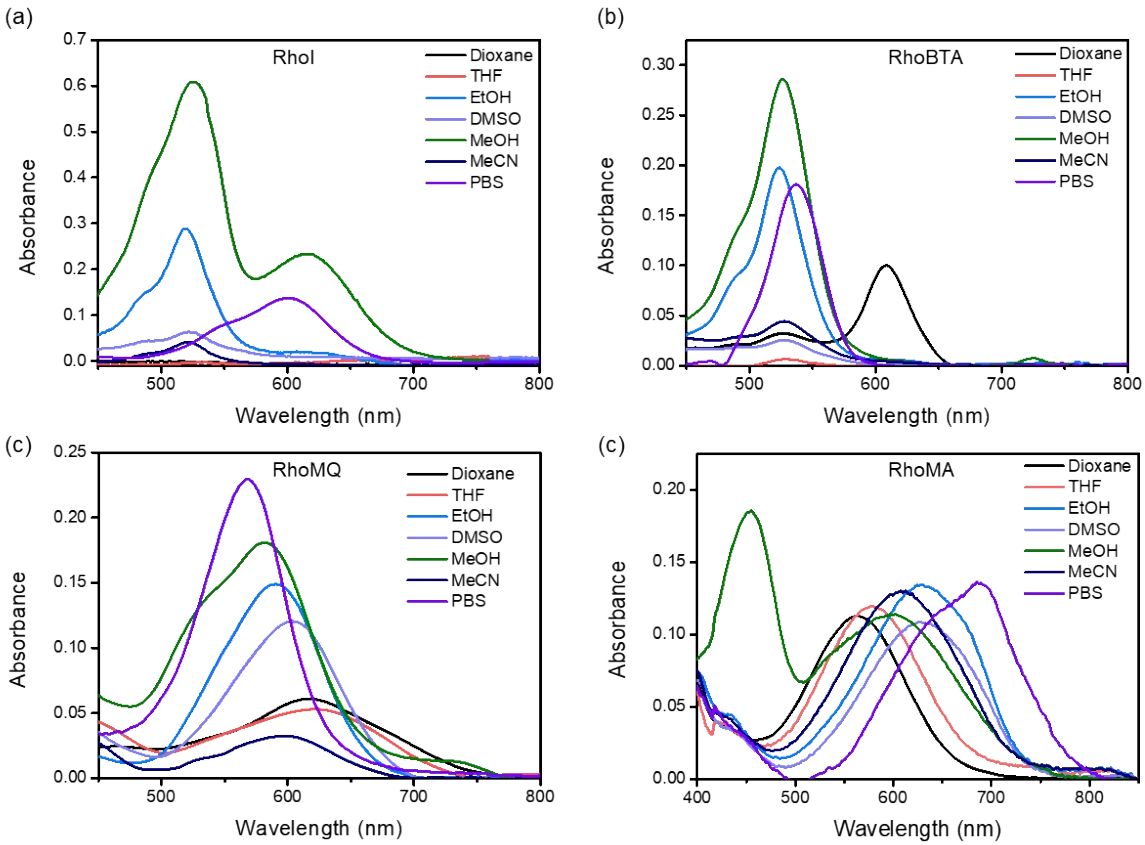

Fig. S1. Absorption spectra of RhoMA (a), RhoBTA (b), RhoMQ (c) and RhoMA (d) in different solvents.

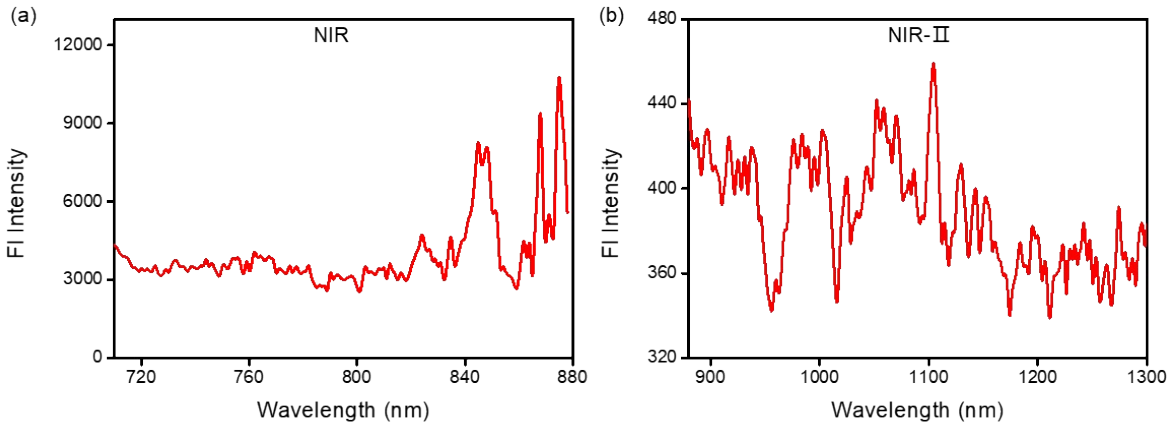

Fig. S2. Fluorescence spectra of RhoMA (5 μM) in pH 7.4 buffer in the NIR (a) and NIR-II (b) fluorescence range.

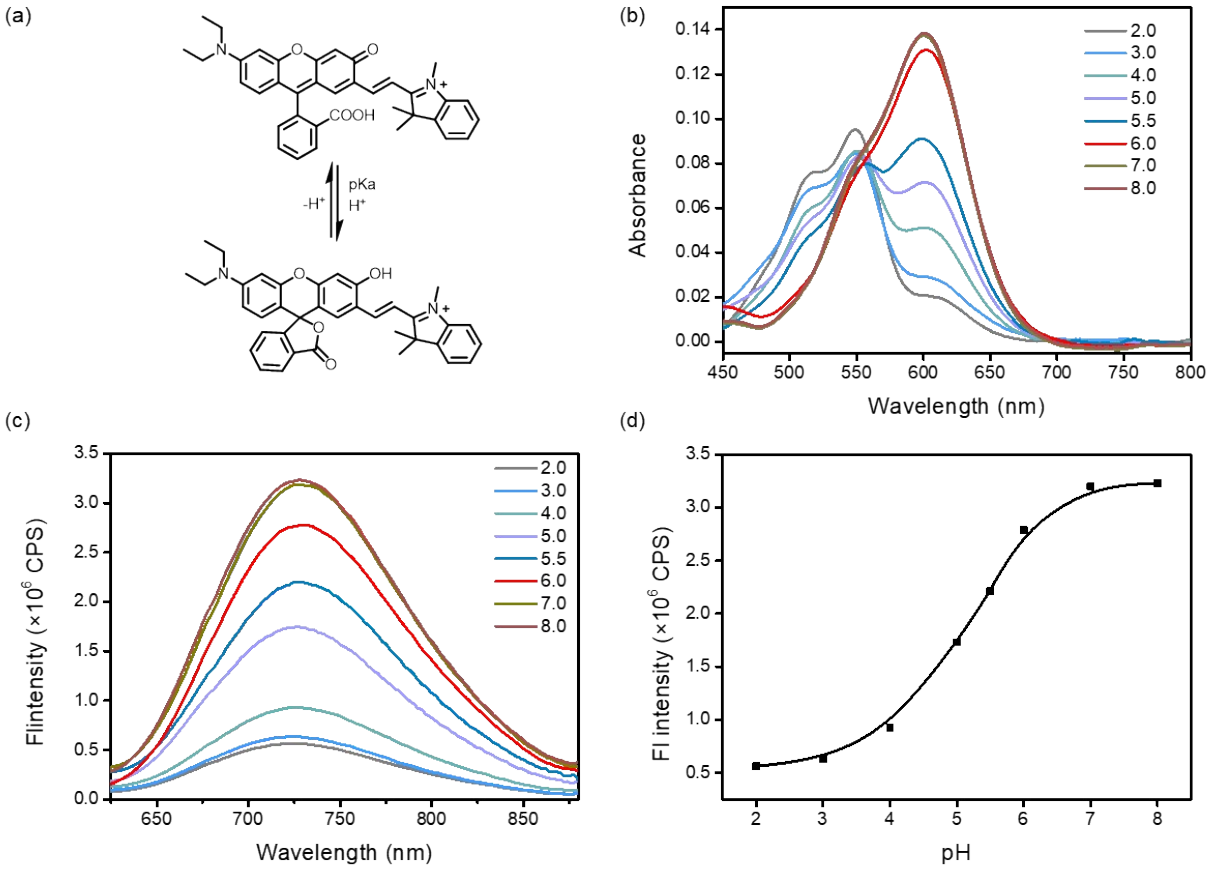

Fig. S3. (a) Acid-base equilibrium of RhoI. Absorption (b) and fluorescence spectra (c) of RhoI (5 μM) in buffers of various pH values. (d) Fluorescence intensities at 727 nm plotted against pH values.

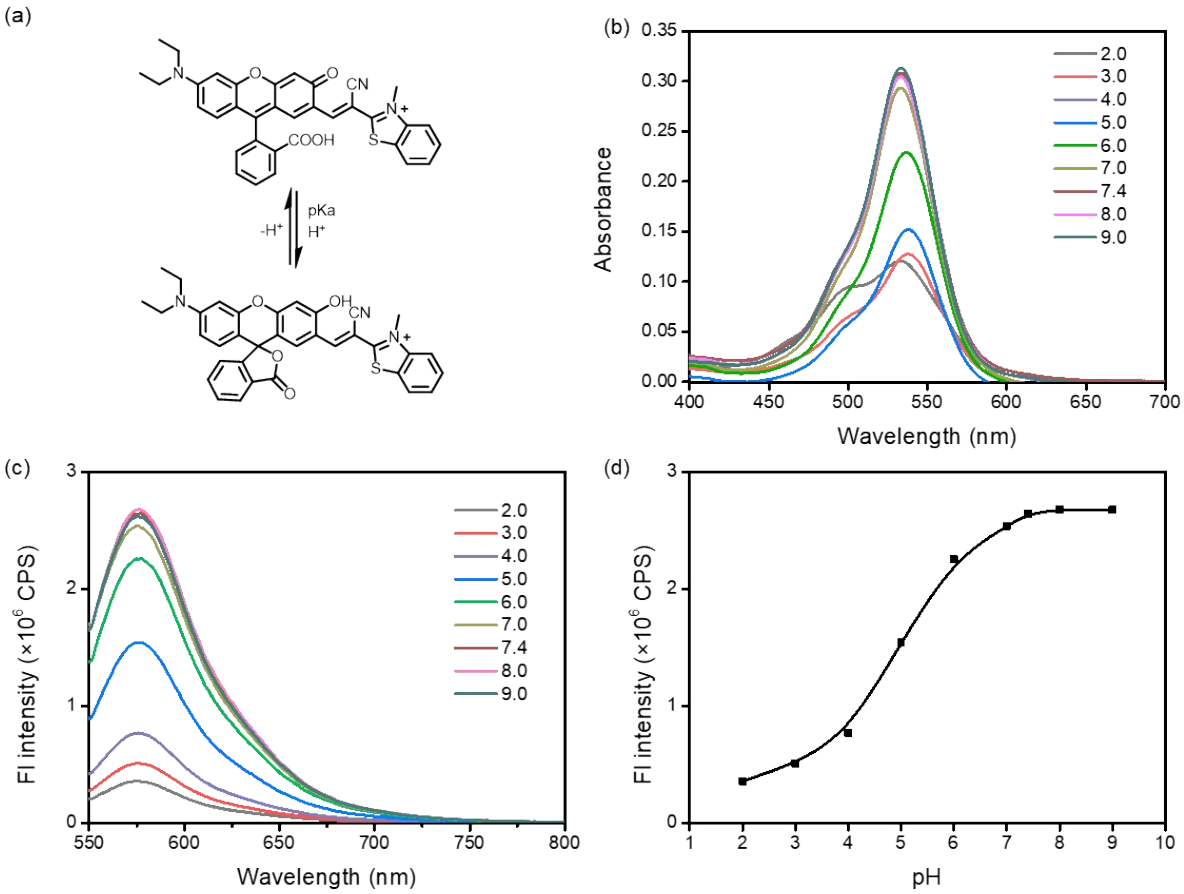

Fig. S4. (a) Acid-base equilibrium of RhoBTA. Absorption (b) and fluorescence spectra (c) of RhoBTA (5 μM) in buffers of various pH values. (d) Fluorescence intensities at 575 nm plotted against pH values.

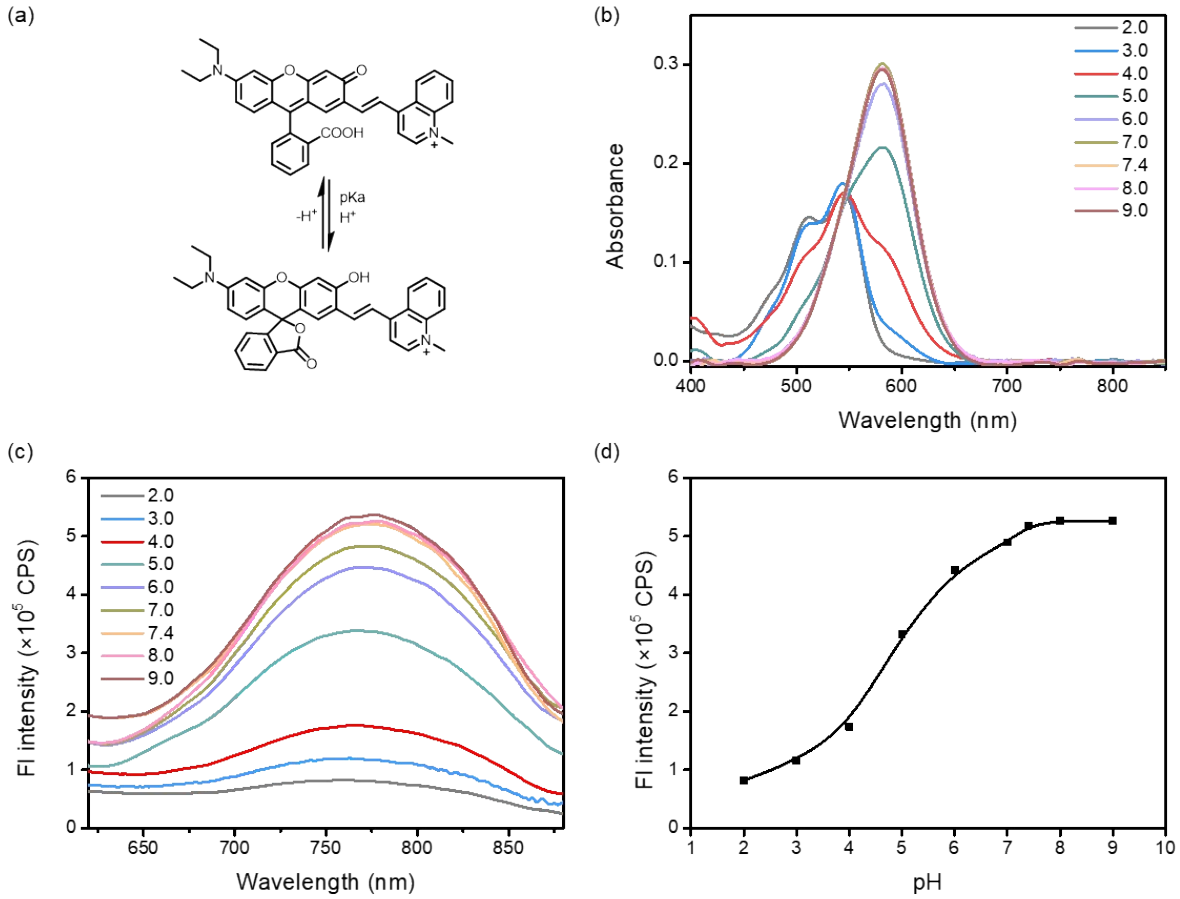

Fig. S5. (a) Acid-base equilibrium of RhoMQ. Absorption (b) and fluorescence spectra (c) of RhoMQ (5 μM) in buffers of various pH values. (d) Fluorescence intensities at 775 nm plotted against pH values.

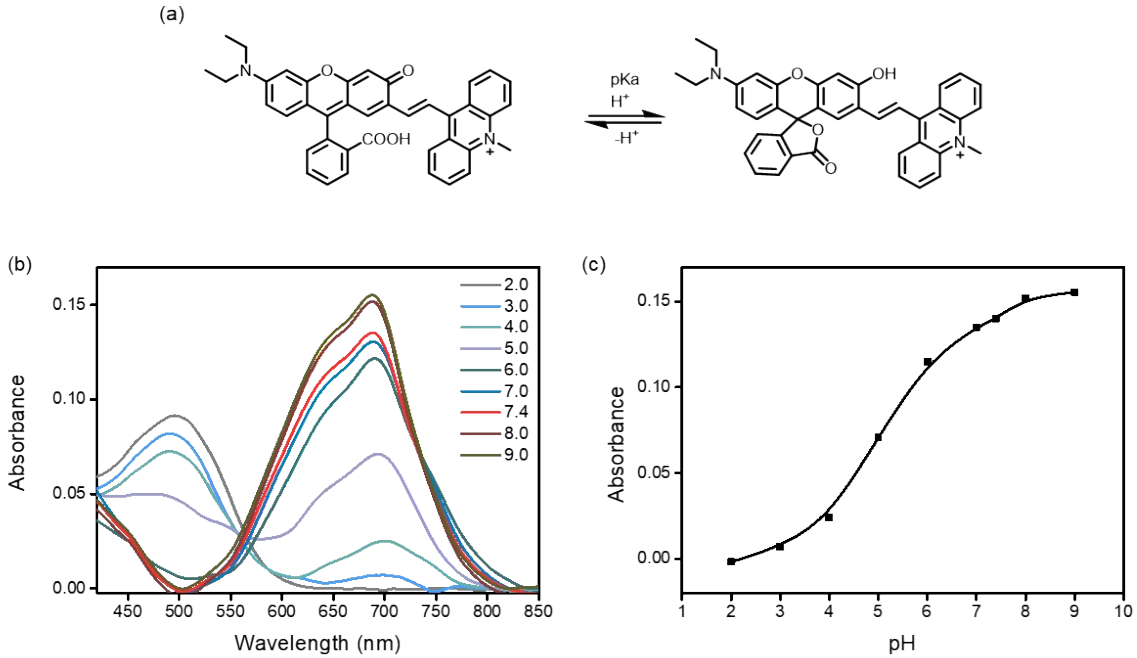

Fig. S6. (a) Acid-base equilibrium of RhoMA. (b) Absorption spectra of RhoMA (5 μM) in buffers of various pH values. (c) Absorbance at 690 nm plotted against pH values.

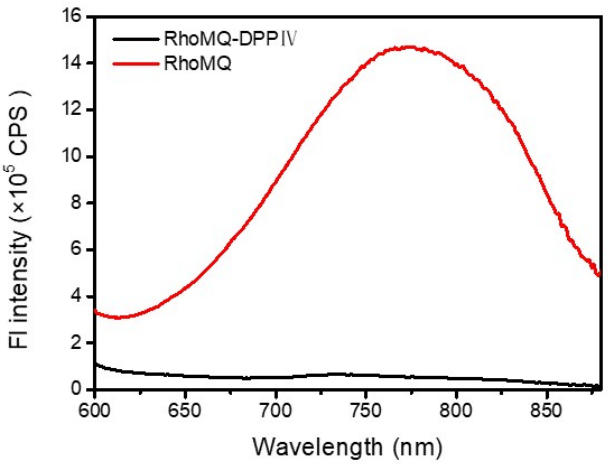

Fig. S7. Fluorescence spectra of RhoMQ-DPPIV (5 μM) and RhoMQ (5 μM) in PBS (10 mM, PH=7.4).

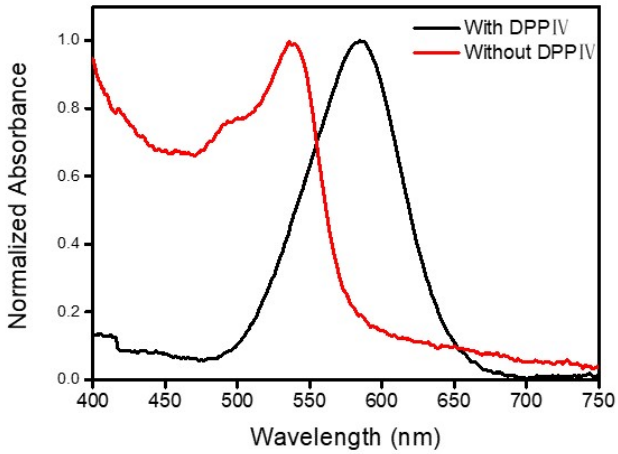

Fig. S8. Absorption spectra of RhoMQ-DPPIV (5 μM) with or without DPPIV (2.0 μg/mL) in PBS (10 mM, PH=7.4).

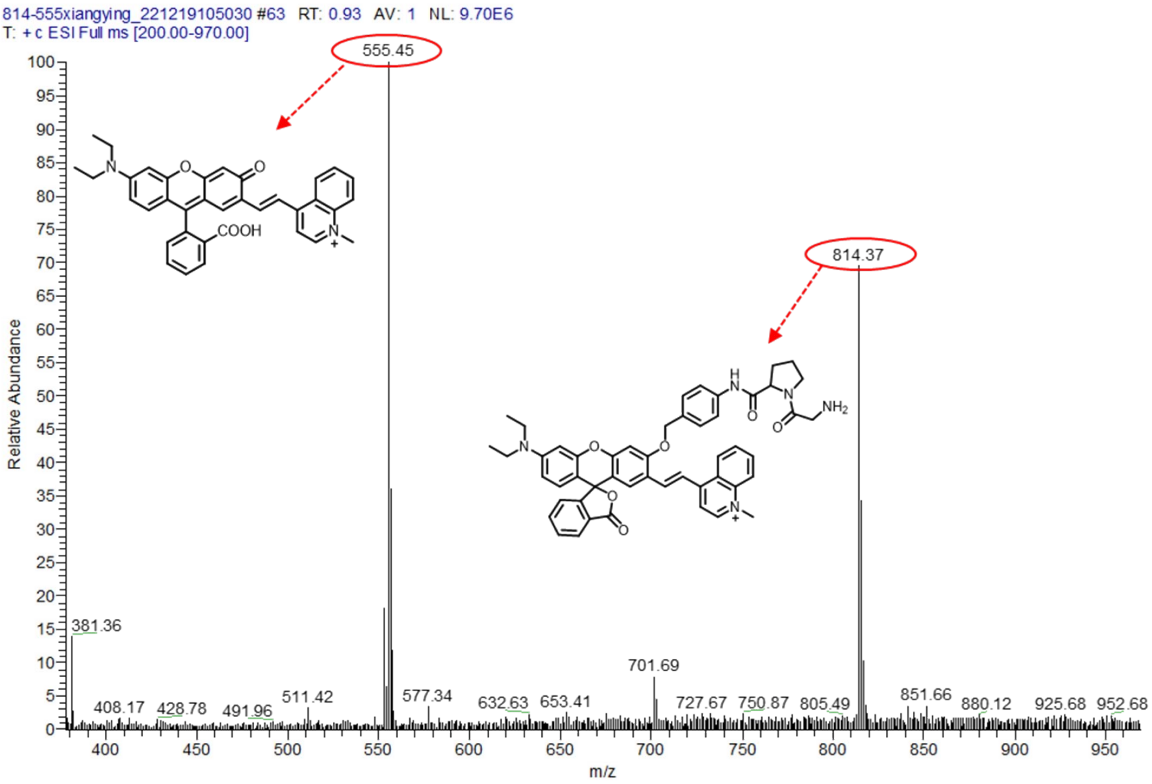

Fig. S9. ESI-MS analysis of the reaction products of DPPIV-catalyzed RhoMQ-DPPIV.

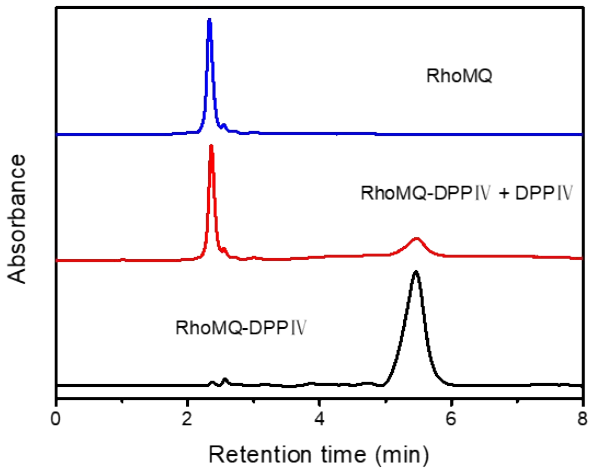

Fig. S10. HPLC analysis of the reaction products of DPPIV-catalyzed RhoMQ-DPPIV.

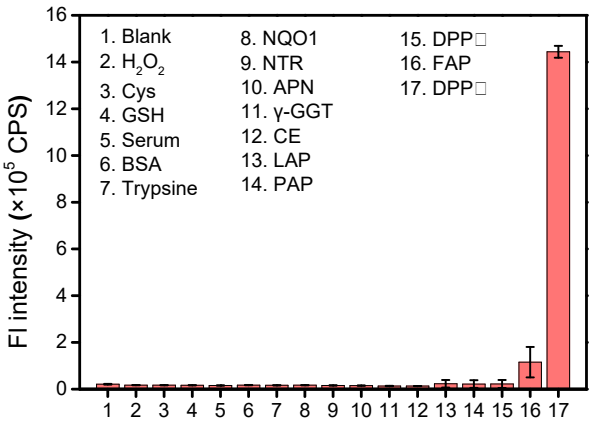

Fig. S11. Fluorescence intensities at 775 nm for RhoMQ-DPPIV (5 μM) in the presence of H_2O_2 (100 μM), Cys (100 μM), GSH (5 mM), serum (20%), BSA (2.0 μg/mL), Trypsine (0.25%), NAD(P)H quinone dehydrogenase 1 (NQO1, 2.0 μg/mL), nitroreductase (NTR, 2.0 μg/mL), APN (2.0 μg/mL), gamma-glutamyl transferase (γ-GGT, 2.0 μg/mL), carboxylesterases (CE, 2.0 μg/mL), leucine aminopeptidase (LAP, 2.0 μg/mL), prolidase (PAP, 2.0 μg/mL), dipeptidyl peptidases VIII (DPP VIII, 2.0 μg/mL), fibroblast activation protein (FAP, 2.0 μg/mL) and DPPIV (2.0 μg/mL) in aqueous solution (PBS/DMSO =9 : 1, v/v, 10 mM, pH = 7.4). Data are presented as the mean ± s.d (n = 3).

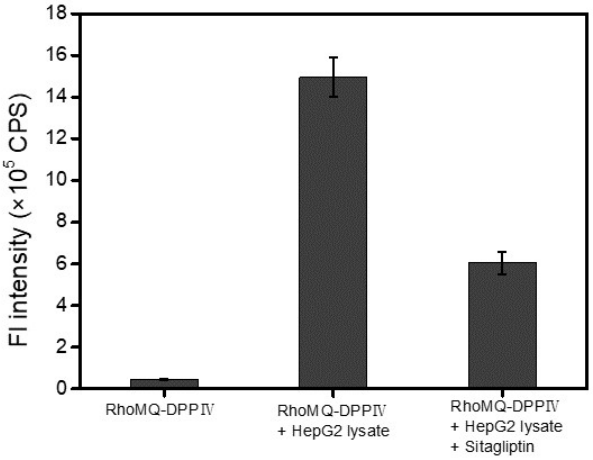

Fig. S12. Fluorescence intensities at 775 nm for RhoMQ-DPPIV (5 μM) in HepG2 cell lysate with or without pretreatment of sitagliptin. Data are presented as the mean ± s.d (n = 3).

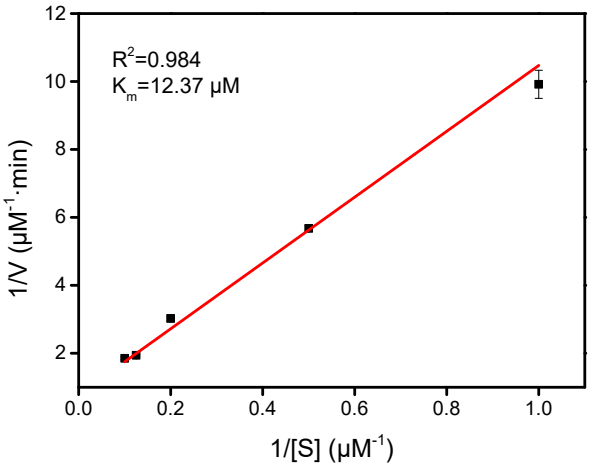

Fig. S13. Line weaver-Burk plot for DPPIV-catalyzed decaging reaction using RhoMQ-DPPIV as the substrate (S). 1/V was plotted against 1/[S]. Data are presented as the mean ± s.d (n = 3).

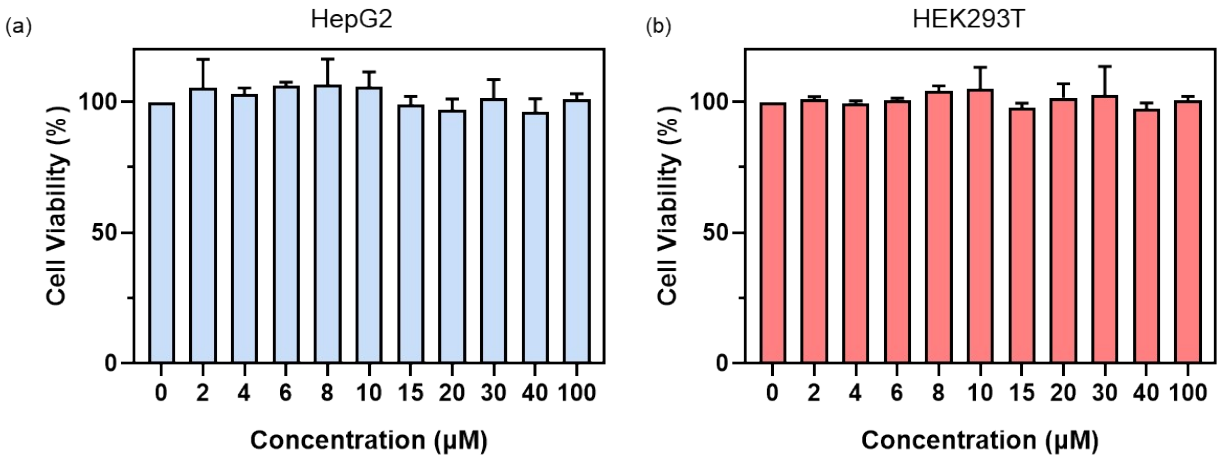

Fig. S14. Cytotoxicity effect of RhoMQ-DPPIV (0 - 100 μM) on HepG2 and HEK293T cells. Data are presented as the mean ± s.d (n = 3).

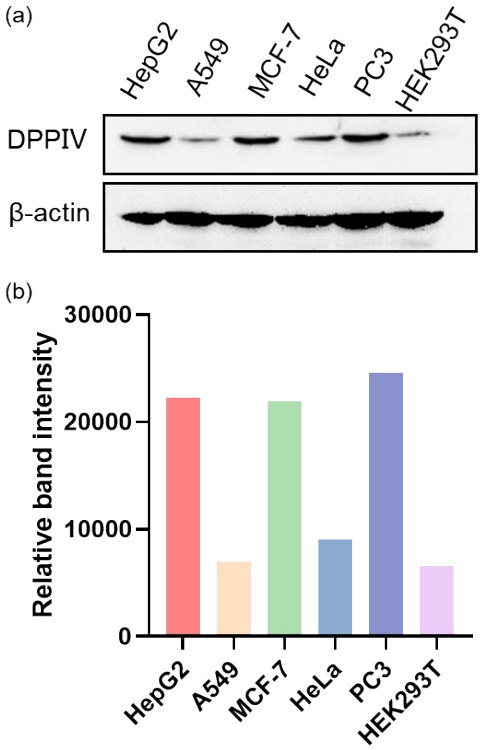

Fig. S15. Western blot (a) and quantitative analysis (b) of DPPIV expression levels in HepG2, A549, MCF-7, HeLa, PC3 and HEK293T cells.

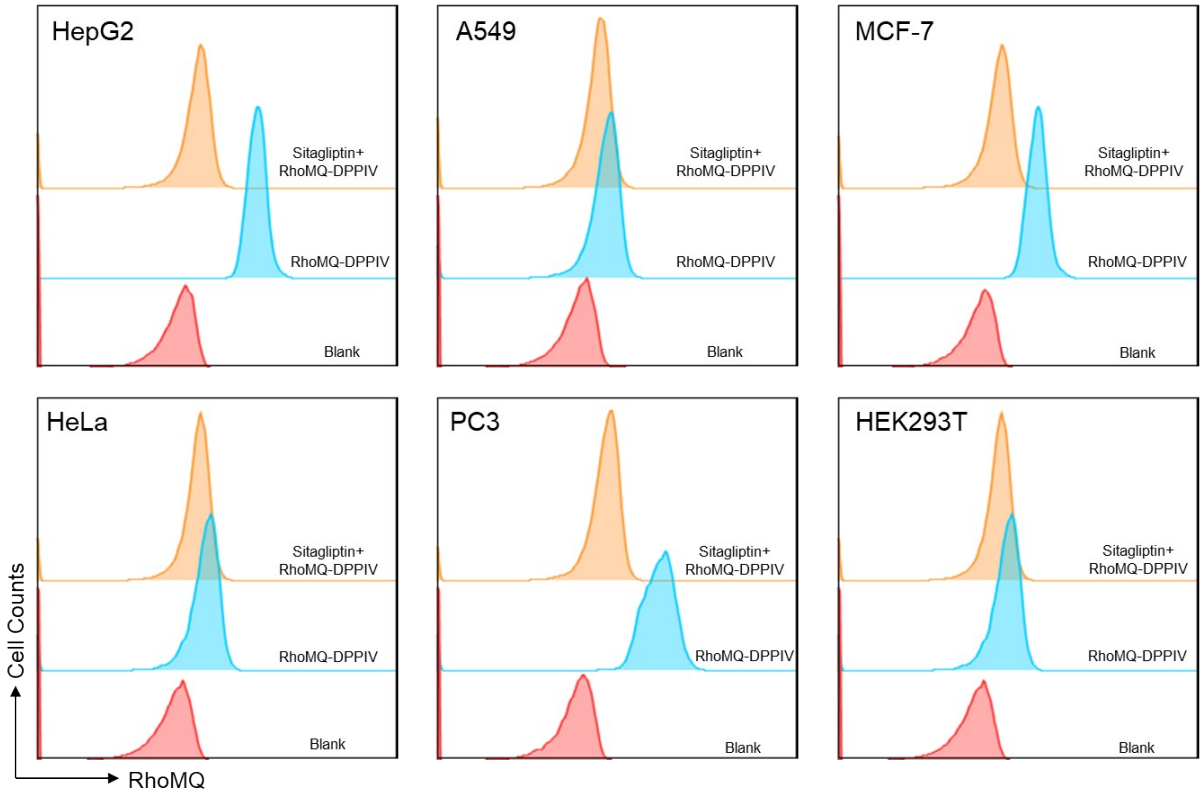

Fig. S16. Flow cytometry profiles for RhoMQ-DPPIV (5 μM) treated cells with or without pretreatment of sitagliptin.

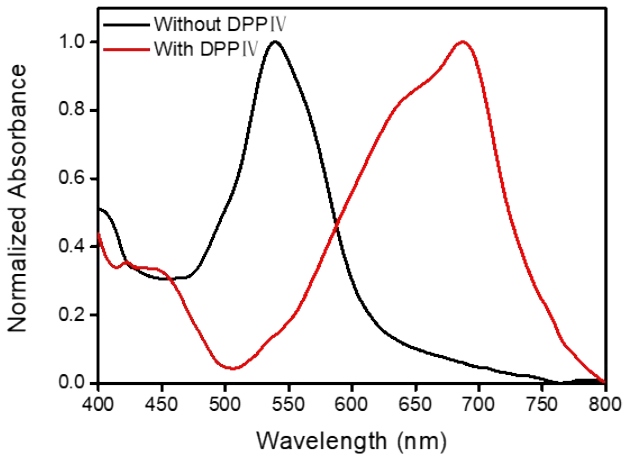

Fig. S17. Absorption spectra of RhoMA-DPPIV (5 μM) with or without DPPIV (2.0 μg/mL) in PBS (10 mM, PH=7.4).

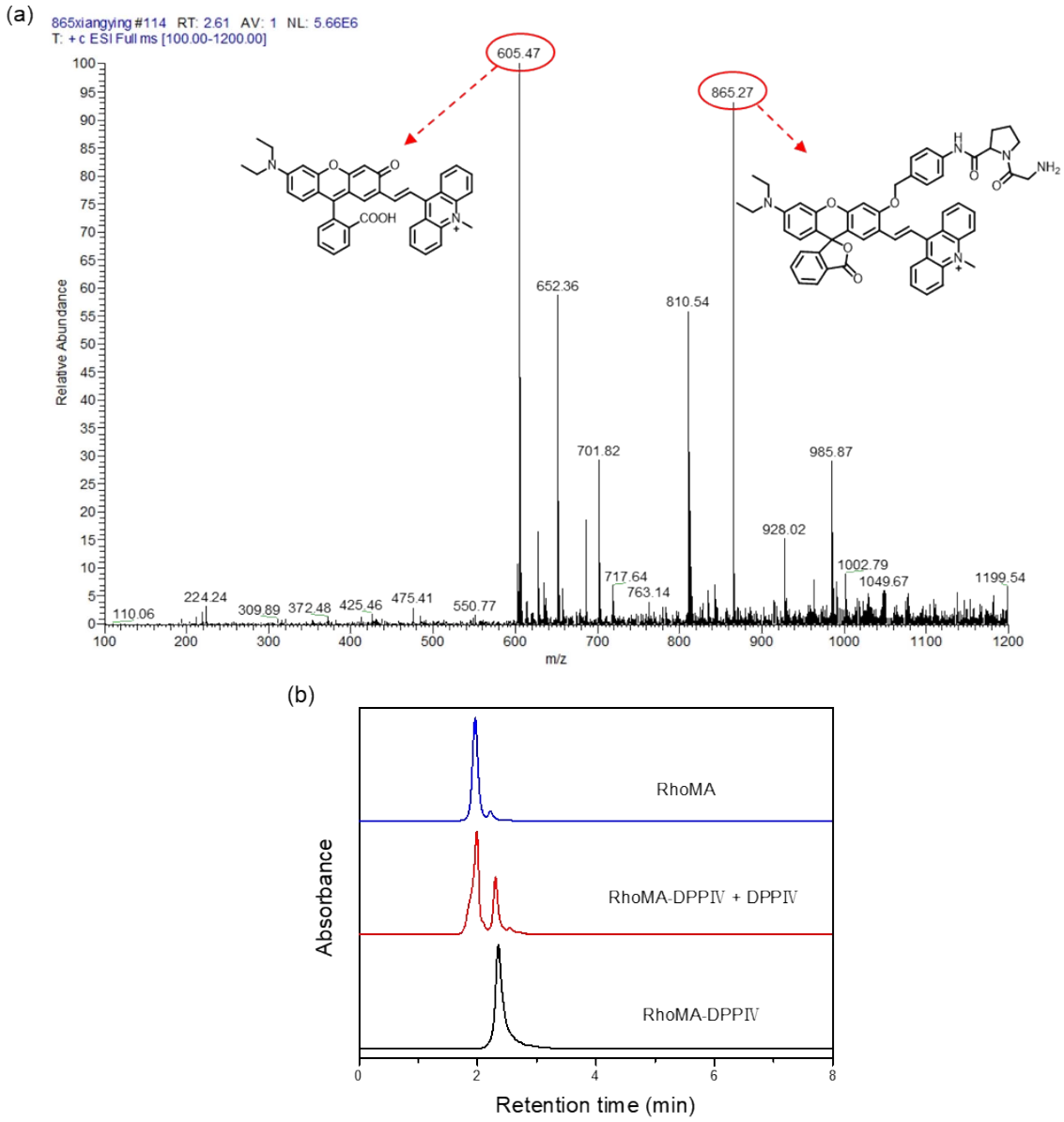

Fig. S18. ESI-MS (a) and HPLC (b) analysis of the reaction products of DPPIV-catalyzed RhoMA-DPPIV.

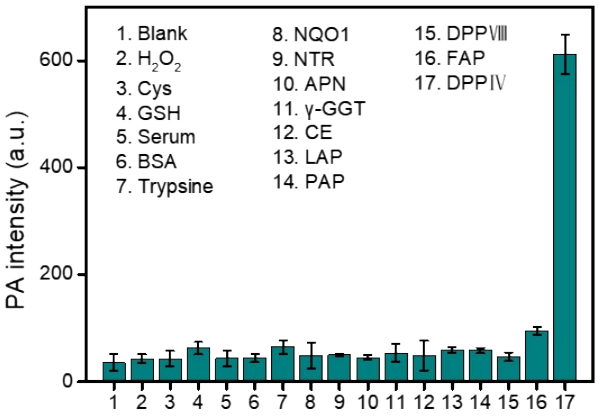

Fig. S19. PA intensities at 690 nm for RhoMA-DPPIV (5 μM) in the prescence of H_2O_2 (100 μM), Cys (100 μM), GSH (5 mM), serum (20%), BSA (2.0 μg/mL), Trypsine (0.25%), NAD(P)H quinone dehydrogenase 1 (NQO1, 2.0 μg/mL), nitroreductase (NTR, 2.0 μg/mL), APN (2.0 μg/mL), gamma-glutamyl transferase (γ-GGT, 2.0 μg/mL), carboxylesterases (CE, 2.0 μg/mL), leucine aminopeptidase (LAP, 2.0 μg/mL), prolidase (PAP, 2.0 μg/mL), dipeptidyl peptidases VIII (DPP VIII, 2.0 μg/mL), fibroblast activation protein (FAP, 2.0 μg/mL) and DPPIV (2.0 μg/mL) in aqueous solution (PBS/DMSO =9 : 1, v/v, 10 mM, pH = 7.4). Data are presented as mean ± SD from three independent experiments.

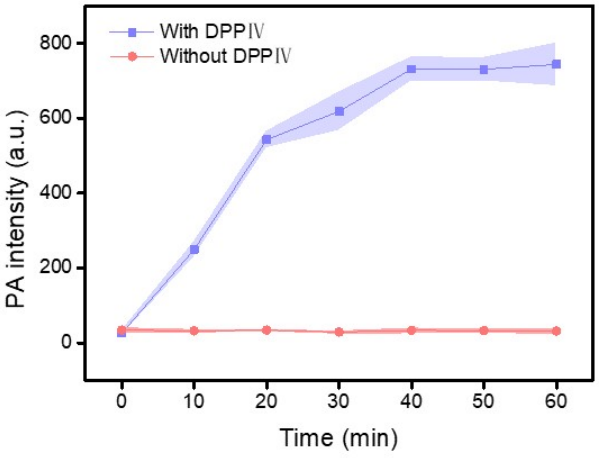

Fig. S20. PA intensities of RhoMA-DPPIV (5 μM) at 690 nm in the presence (purple) and absence (red) of DPPIV (2 μg/mL) as a function of time. Data are presented as the mean ± SD of three independent experiments.

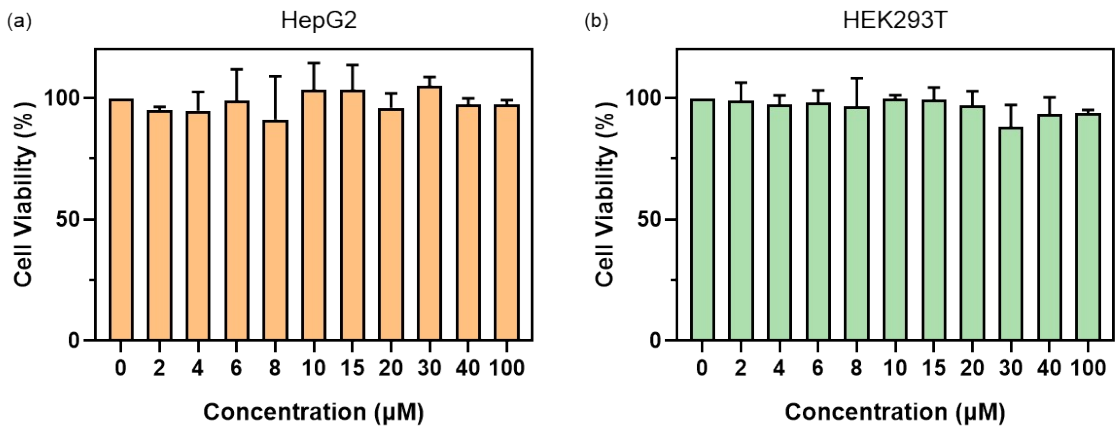

Fig. S21. Cytotoxicity effect of RhoMA-DPPIV (0 -100 μM) on HepG2 and HEK293T cells. Data are presented as the mean ± s.d (n = 3).

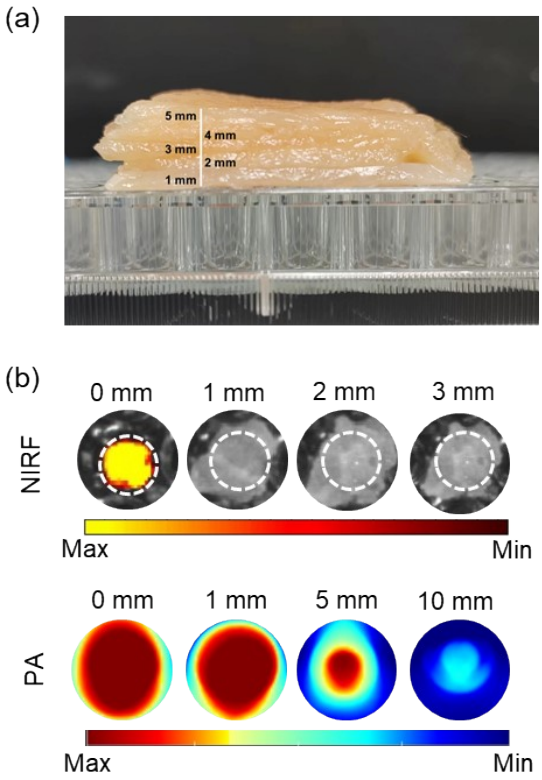

Fig. S22. NIRF images of RhoMQ-DPPIV (5 μM) and PA images of RhoMA-DPPIV (5 μM) treated with DPPIV embedded by different slices of chicken breast tissue. The thickness of one slice chicken breast tissue is around 1 mm.

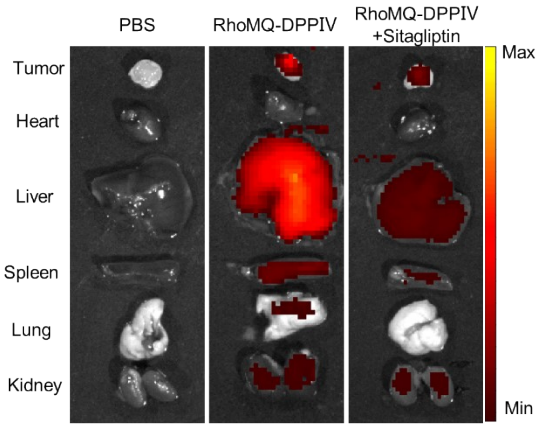

Fig. S23. Representative ex vivo NIRF imaging of dissected tumors and major organs at 3 h post injection of RhoMQ-DPPIV (100 μM in 100 μL PBS) via tail vein. To inhibit DPPIV activity, HepG2 tumor-bearing mice were pre-injected with sitagliptin (100 μM in 100 μL PBS) before tail-vein injection of RhoMQ-DPPIV.

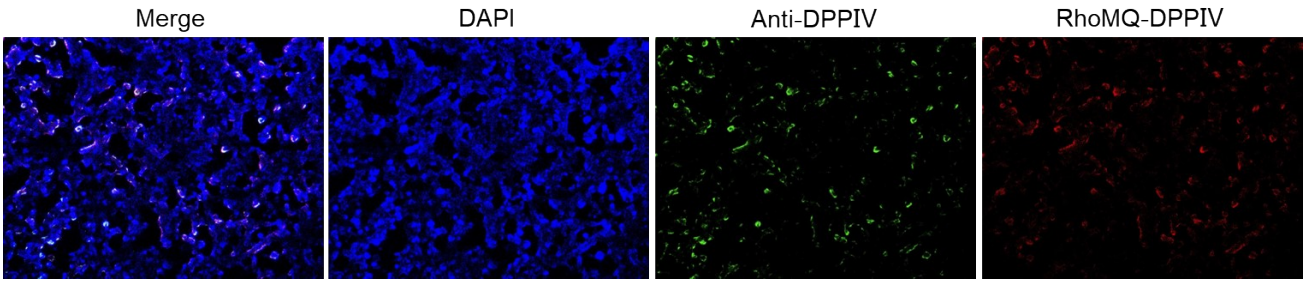

Fig. S24. Colocalization assay for tumor slices treated with RhoMQ-DPPIV and immunofluorescence for DPPIV. Green fluorescence indicated immunofluorescence of DPPIV and red fluorescence indicated activated RhoMQ-DPPIV.

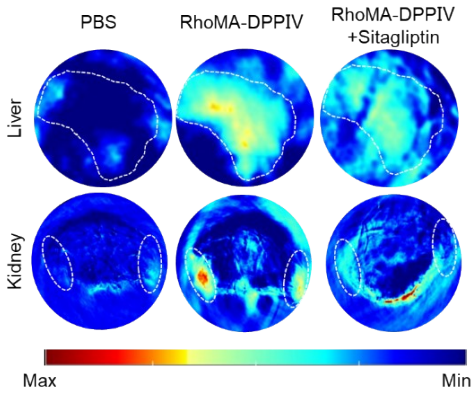

Fig. S25. Representative ex vivo PA imaging of dissected liver and kidney organs at 3 h post-injection of RhoMA-DPPIV (100 μM in 100 μL PBS) via tail vein. To inhibit DPPIV activity, HepG2 tumor-bearing mice were pre-injected with sitagliptin (100 μM in 100 μL PBS) before tail-vein injection of RhoMQ-DPPIV.

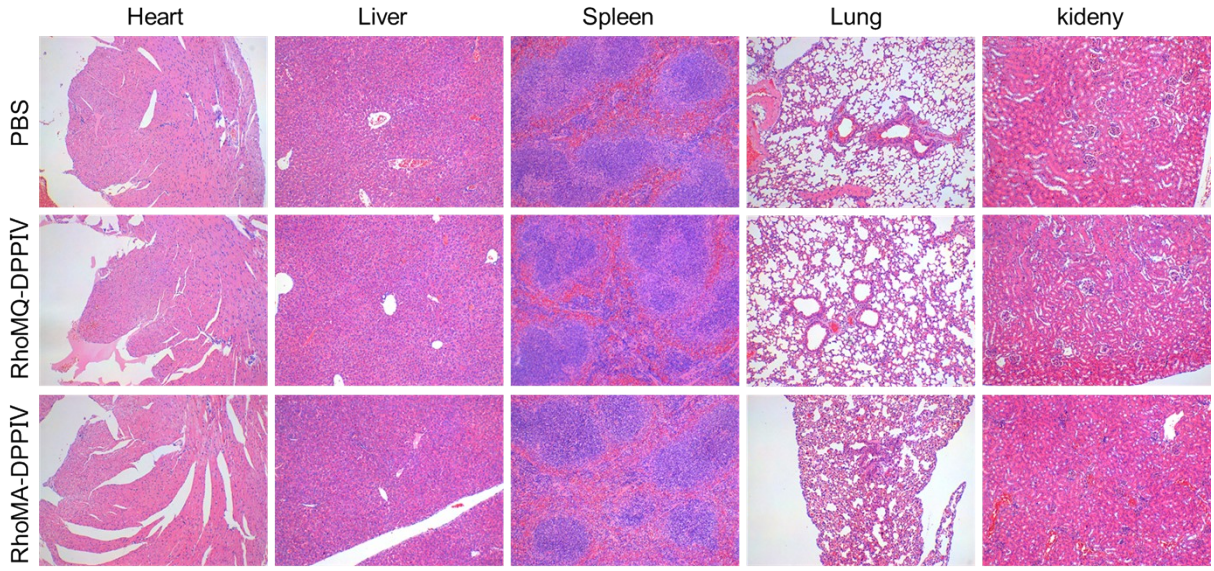

Fig. S26. H&E staining of tissue slices from dissected major organs (heart, liver, spleen, lung and kidney) of HepG2 tumor-bearing mice treated with PBS, RhoMQ-DPPIV and RhoMA-DPPIV via tail-vein injection.

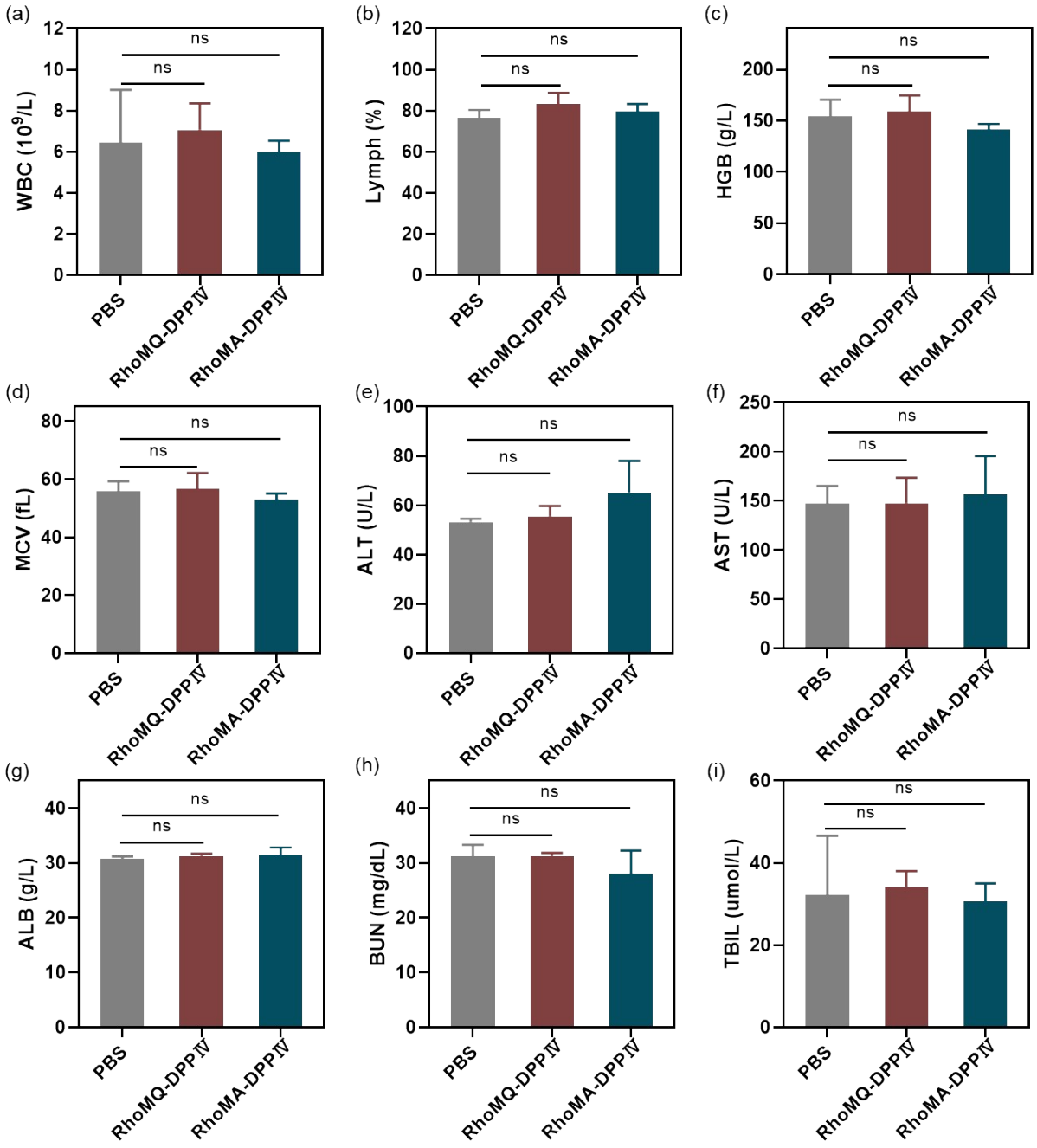

Fig. S27. (a-i) The effects of PBS, RhoMQ-DPPIV and RhoMA-DPPIV on the physiological indicators of white blood cells (WBC), percentage of lymphocytes (Lymph (%)), hemoglobin (HGB), mean corpuscular volume (MCV), alanine aminotransferase (ALT), aspartate aminotransferase (AST), albumin (ALB), blood urea nitrogen (BUN), total bilirubin (TIBL). Statistical comparison was performed by two-tailed t-test (****$p < 0.0001$, **$p < 0.01$, *$p < 0.05$, $n = 3$).

3. Supplementary table

Table S1. The summary of photophysical properties of the four dyes in pH 7.4 buffer.

Probe	λ_{abs}/nm	λ_{em}/nm	pk_{cycl}	$\varepsilon/M^{-1}\,cm^{-1}$	Φ (%)
RhoI	600	727	5.1	3.08×10^5	8.8
RhoBTA	536	575	5.0	1.92×10^5	12.6
RhoMQ	580	775	4.5	1.99×10^5	2.6
RhoMA	690	—	5.2	0.27×10^5	—

4. NMR and MS spectra

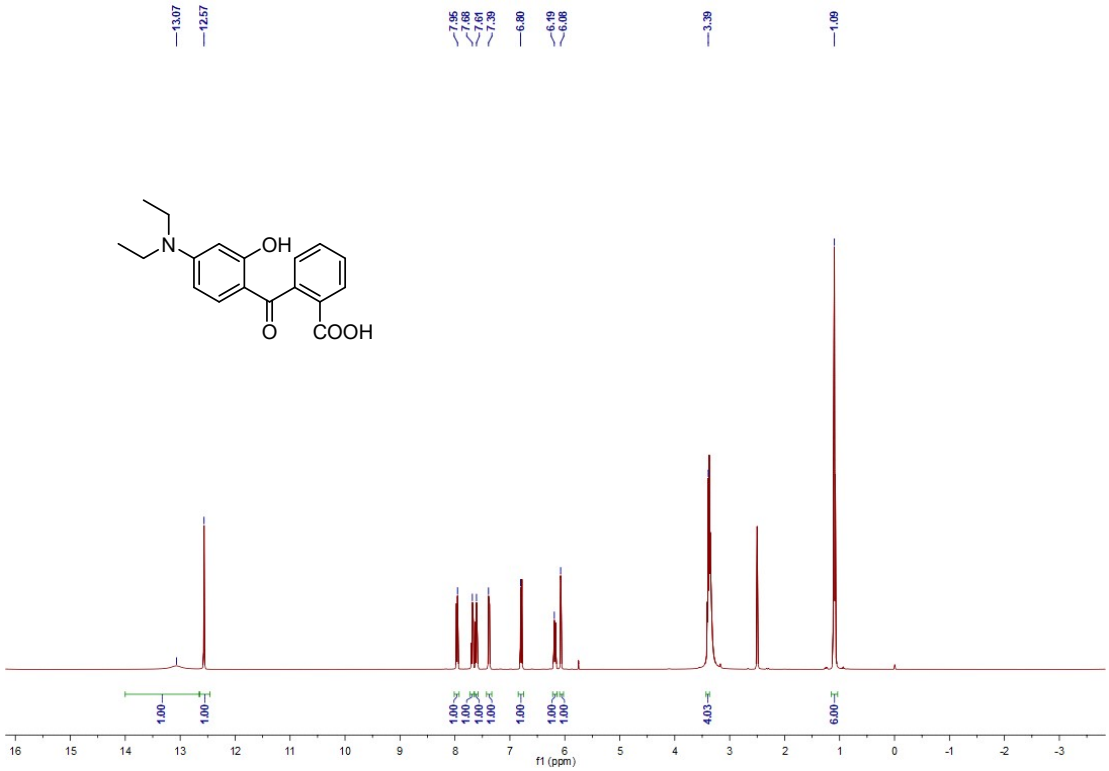

Fig. S28. ^{1}H NMR (400 MHz, 298 K, DMSO-d_6) spectrum for compound **1**.

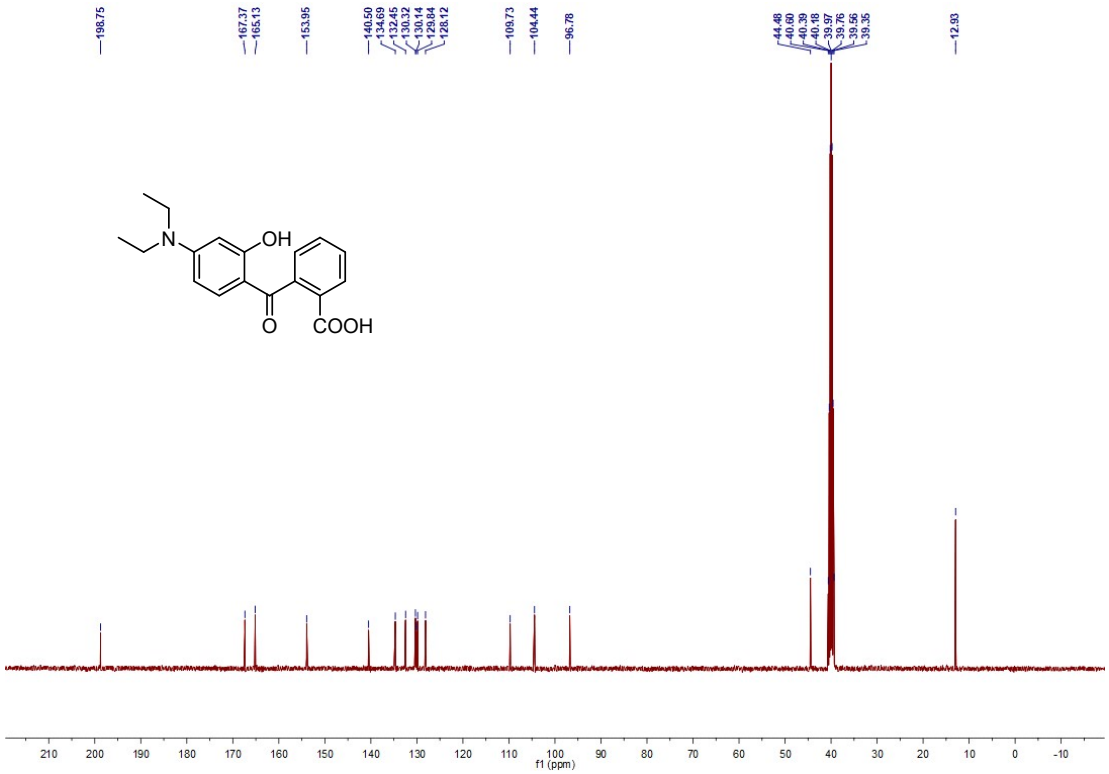

Fig. S29. ^{13}C NMR (100 MHz, 298 K, DMSO-d_6) spectrum for compound **1**.

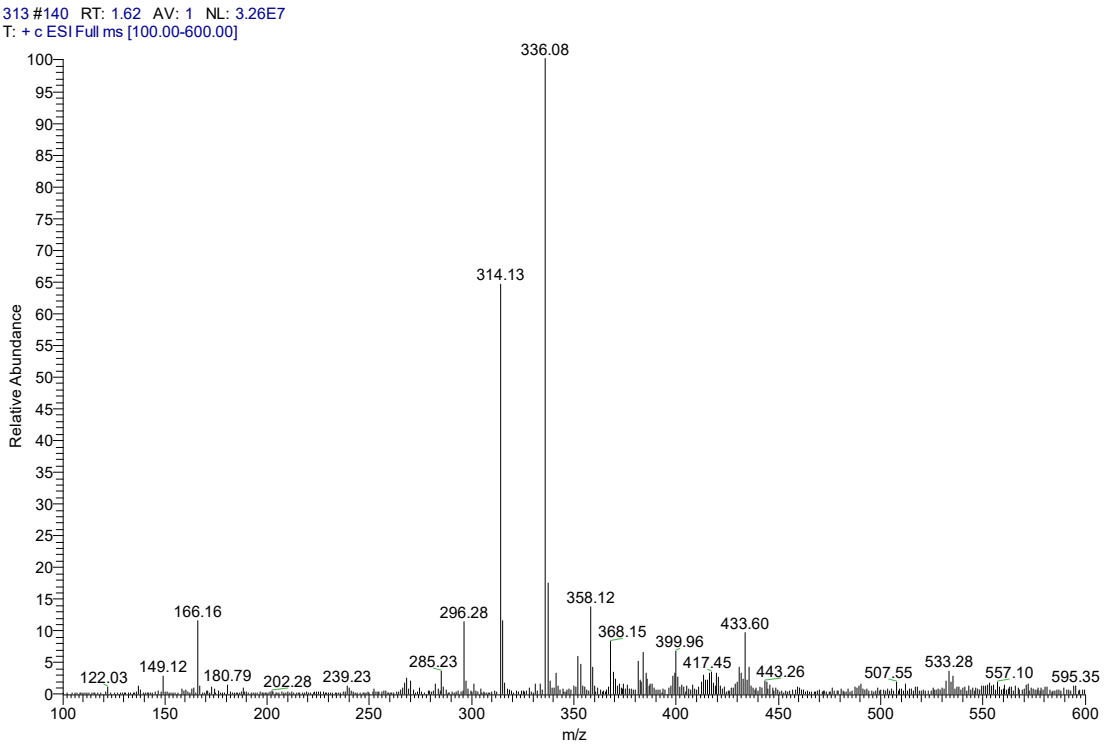

Fig. S30. HR-MS-ESI spectrum for compound **1**.

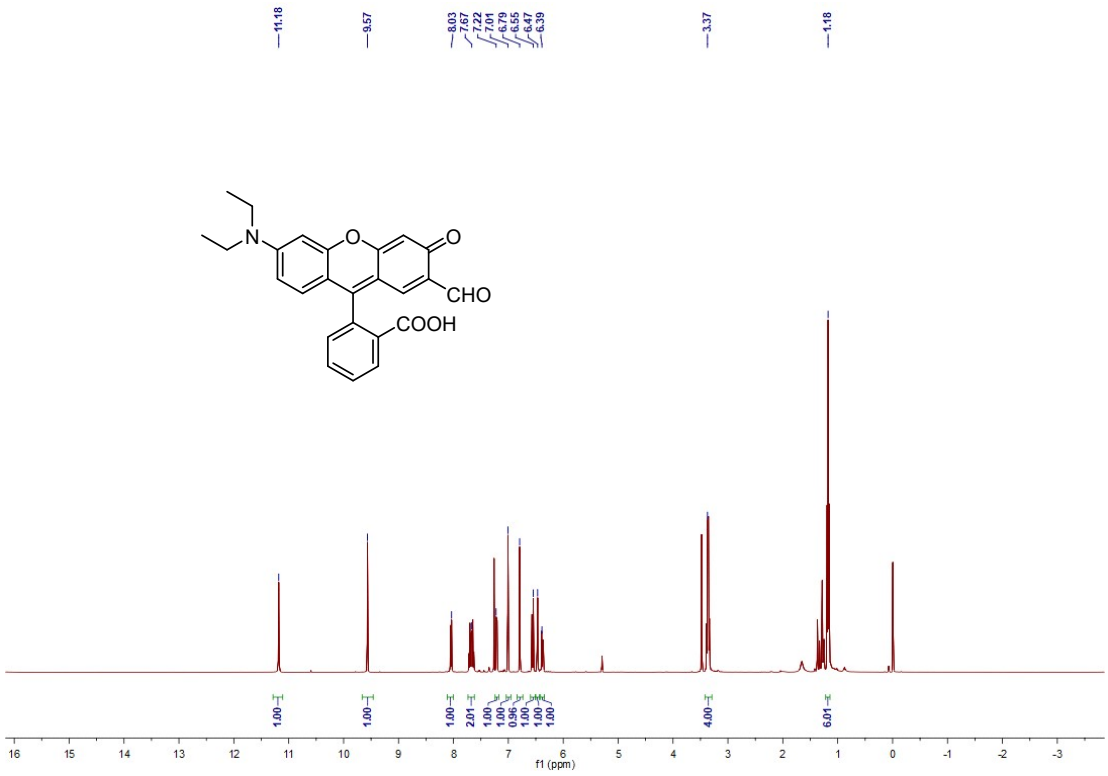

Fig. S31. ^{1}H NMR (400 MHz, 298 K, $CDCl_3$) spectrum for compound **Rho-A**.

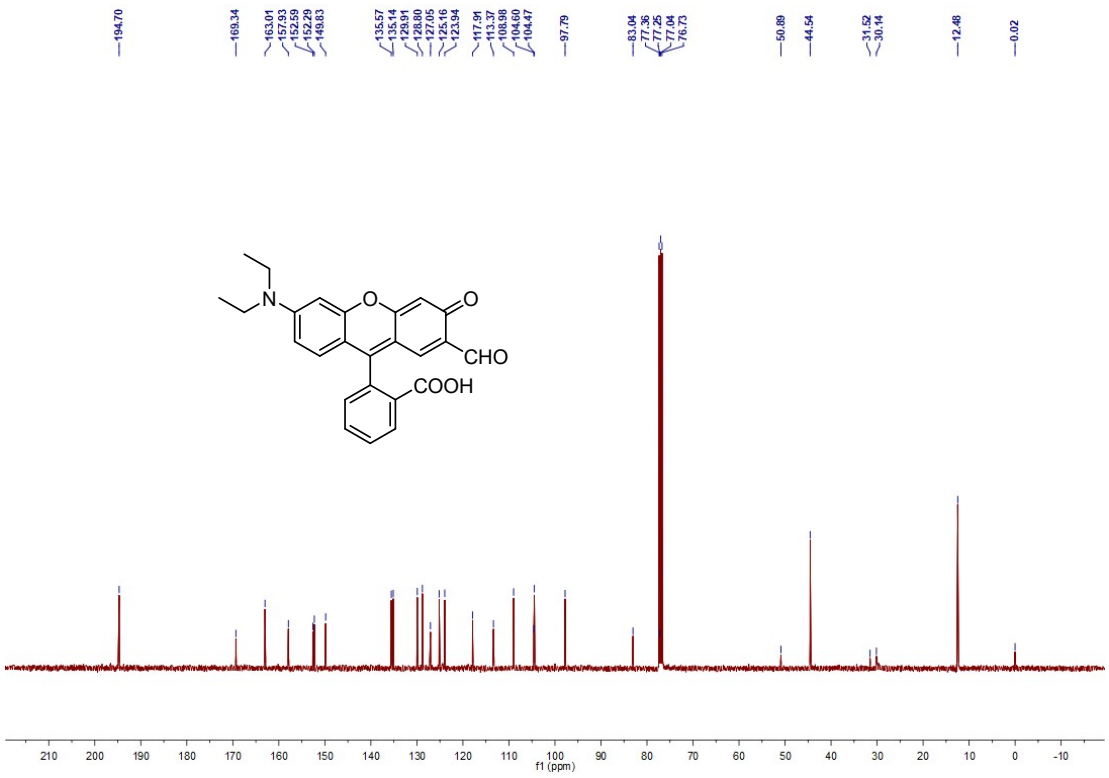

Fig. S32. ^{13}C NMR (100 MHz, 298 K, $CDCl_3$) spectrum for compound **Rho-A**.

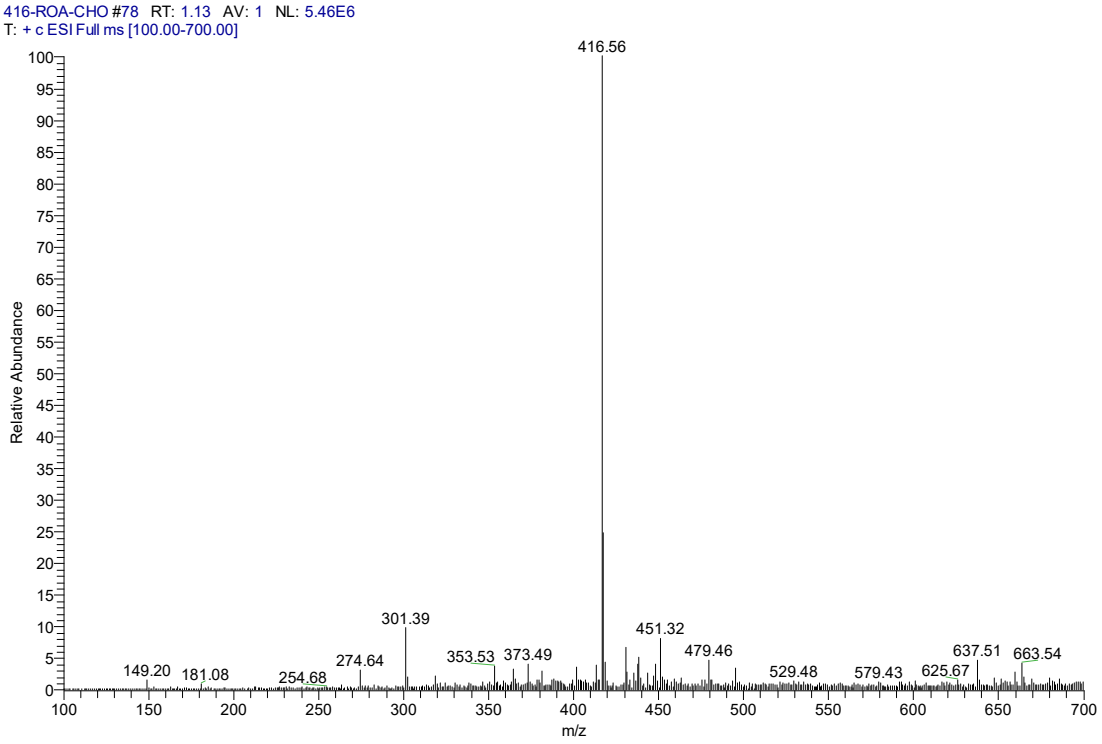

Fig. S33. MS-ESI spectrum for compound **Rho-A**.

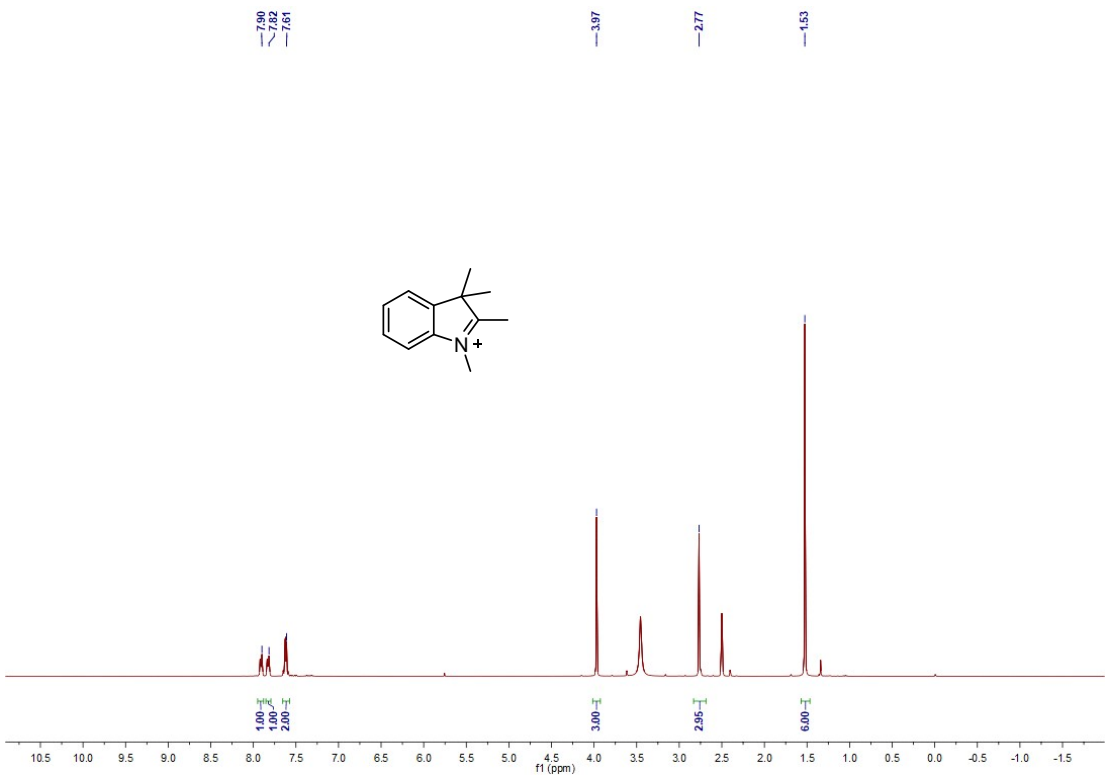

Fig. S34. ^{1}H NMR (400 MHz, 298 K, DMSO-d_6) spectrum for compound **2**.

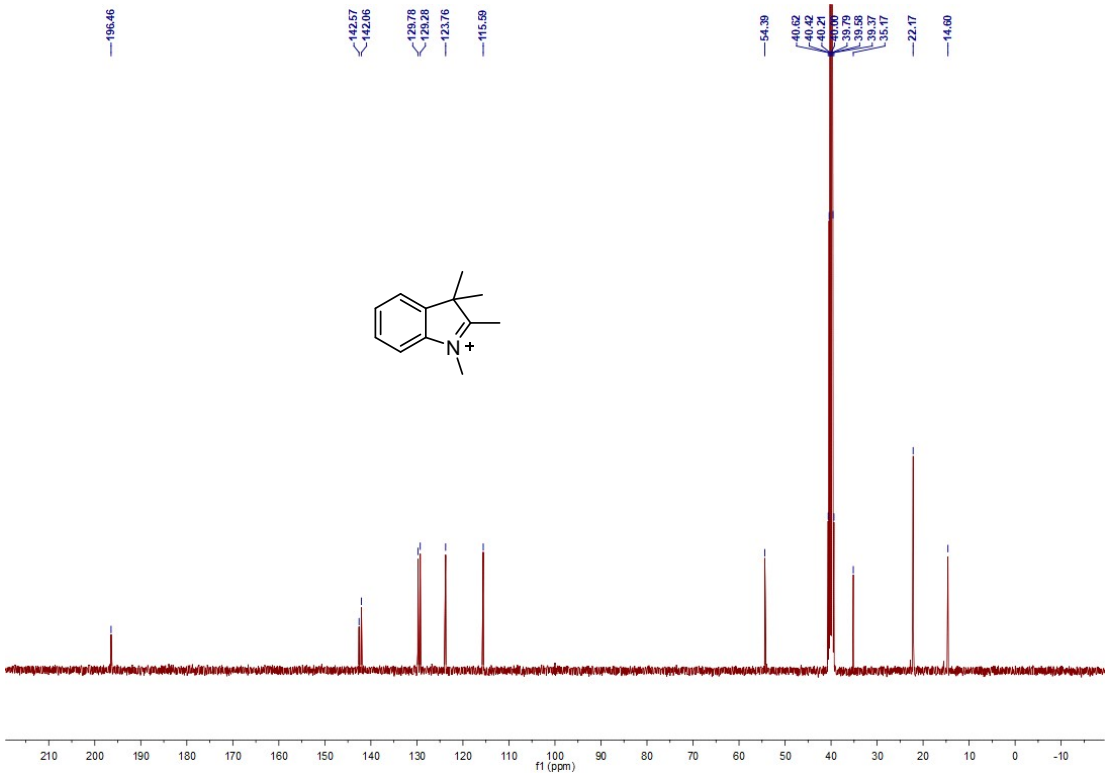

Fig. S35. ^{13}C NMR (100 MHz, 298 K, DMSO-d_6) spectrum for compound **2**.

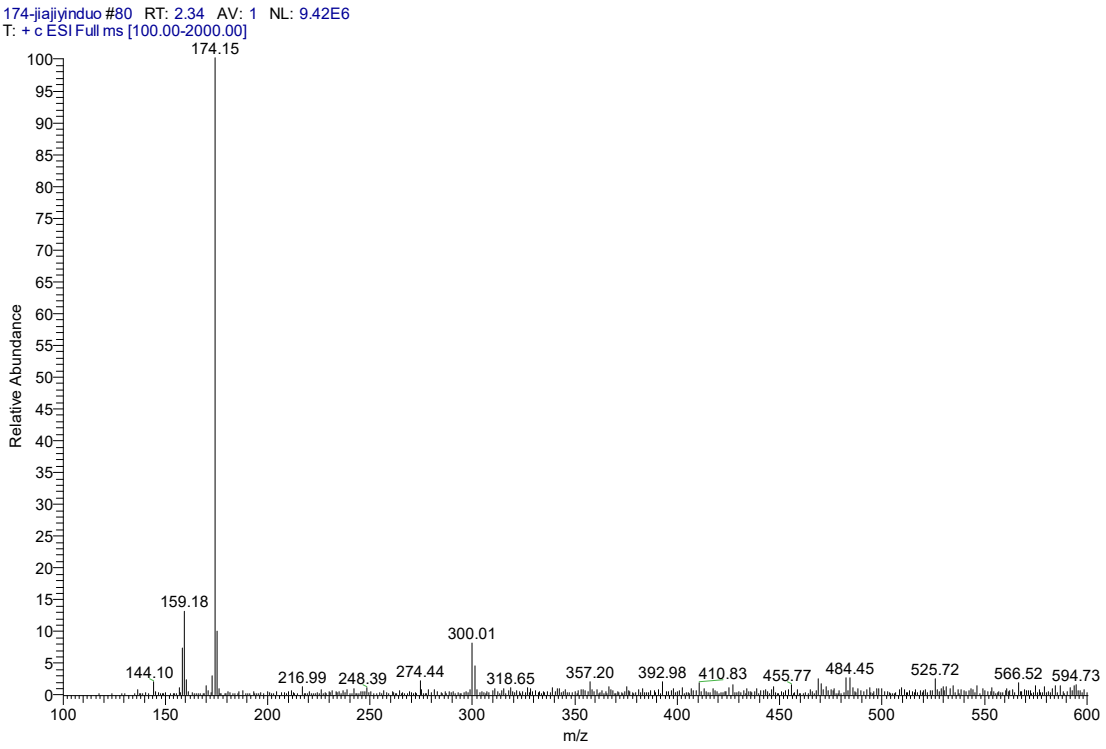

Fig. S36. MS-ESI spectrum for compound **2**.

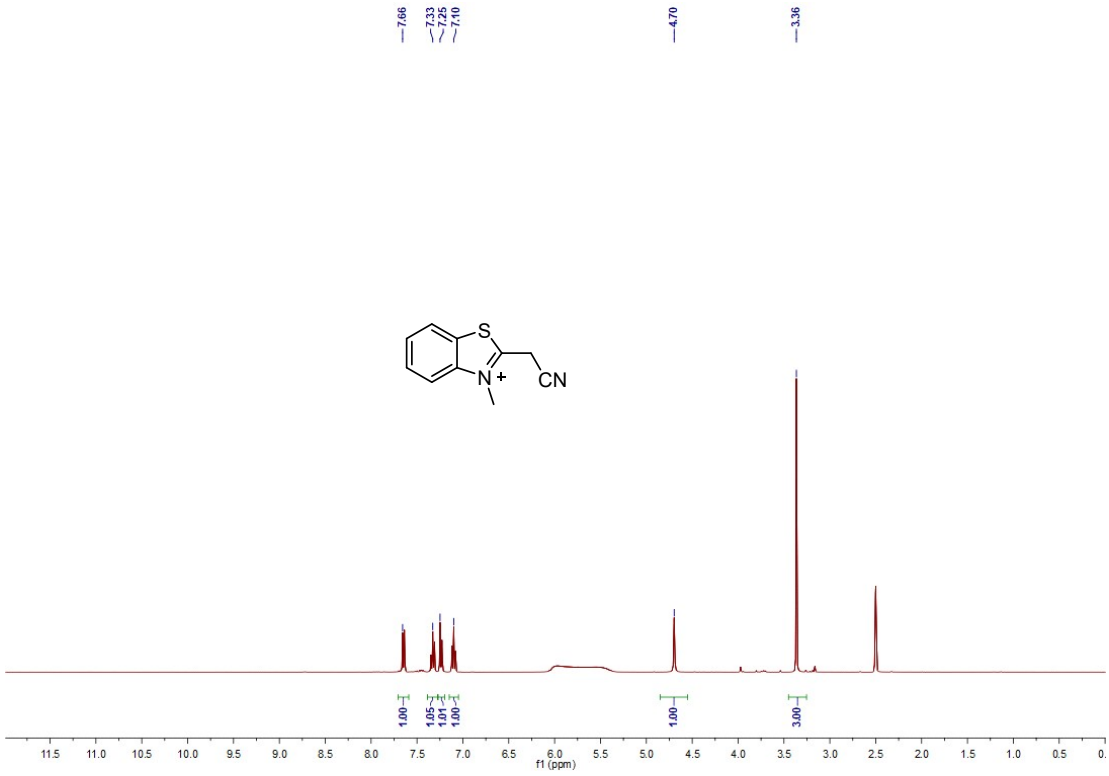

Fig. S37. ^{1}H NMR (400 MHz, 298 K, DMSO-d_6) spectrum for compound **3**.

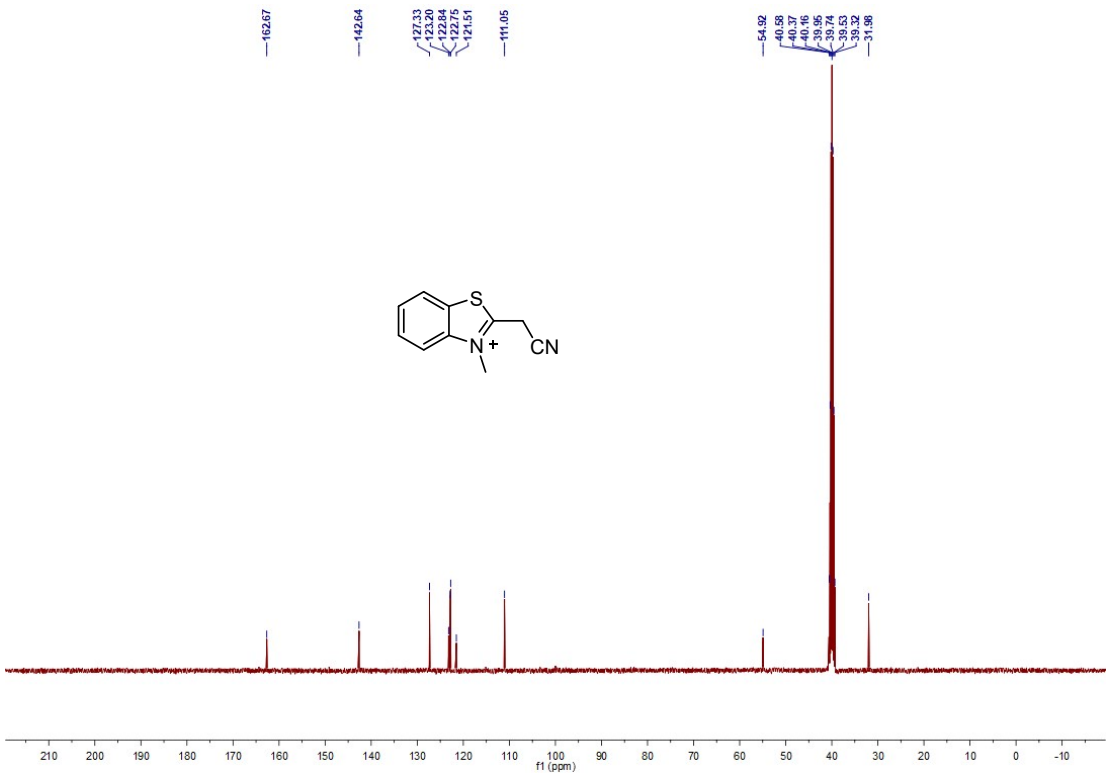

Fig. S38. ^{13}C NMR (100 MHz, 298 K, DMSO-d_6) spectrum for compound **3**.

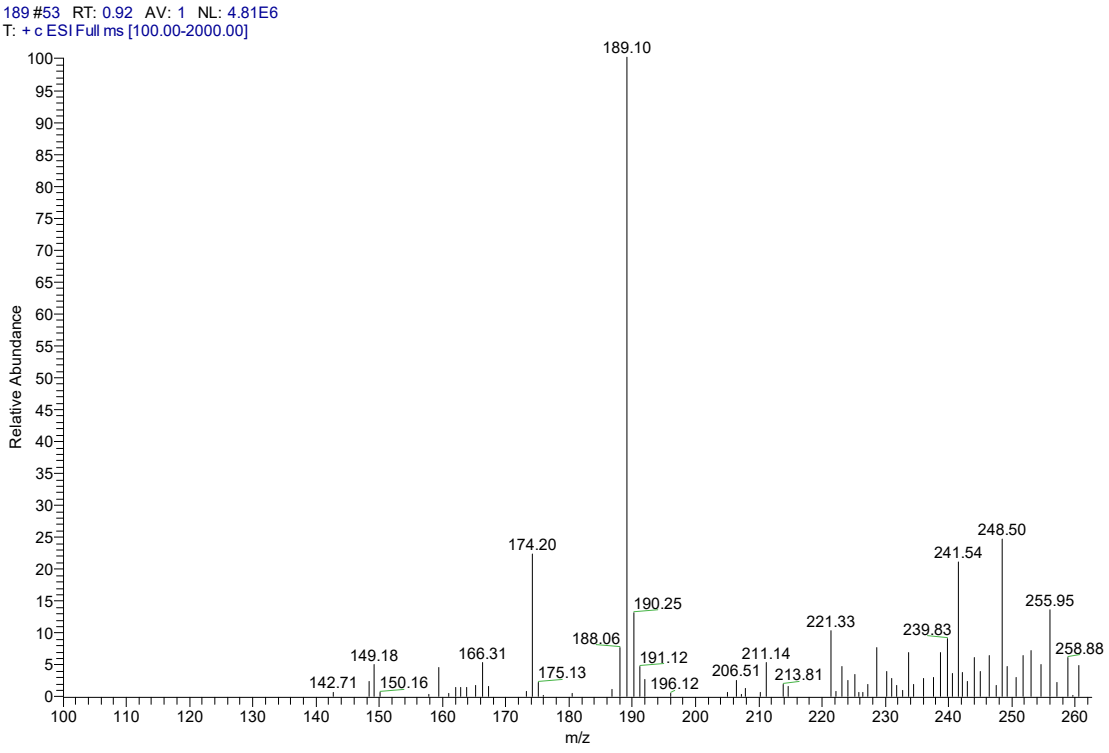

Fig. S39. MS-ESI spectrum for compound **3**.

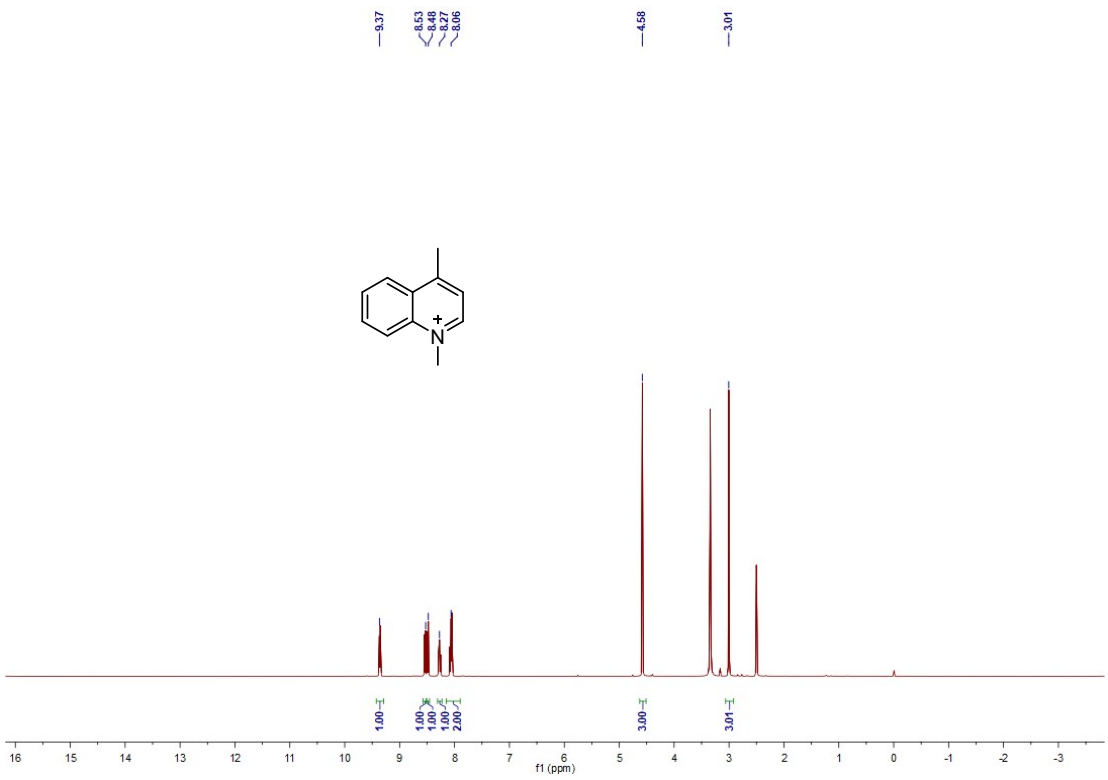

Fig. S40. [1]H NMR (400 MHz, 298 K, DMSO-d_6) spectrum for compound **4**.

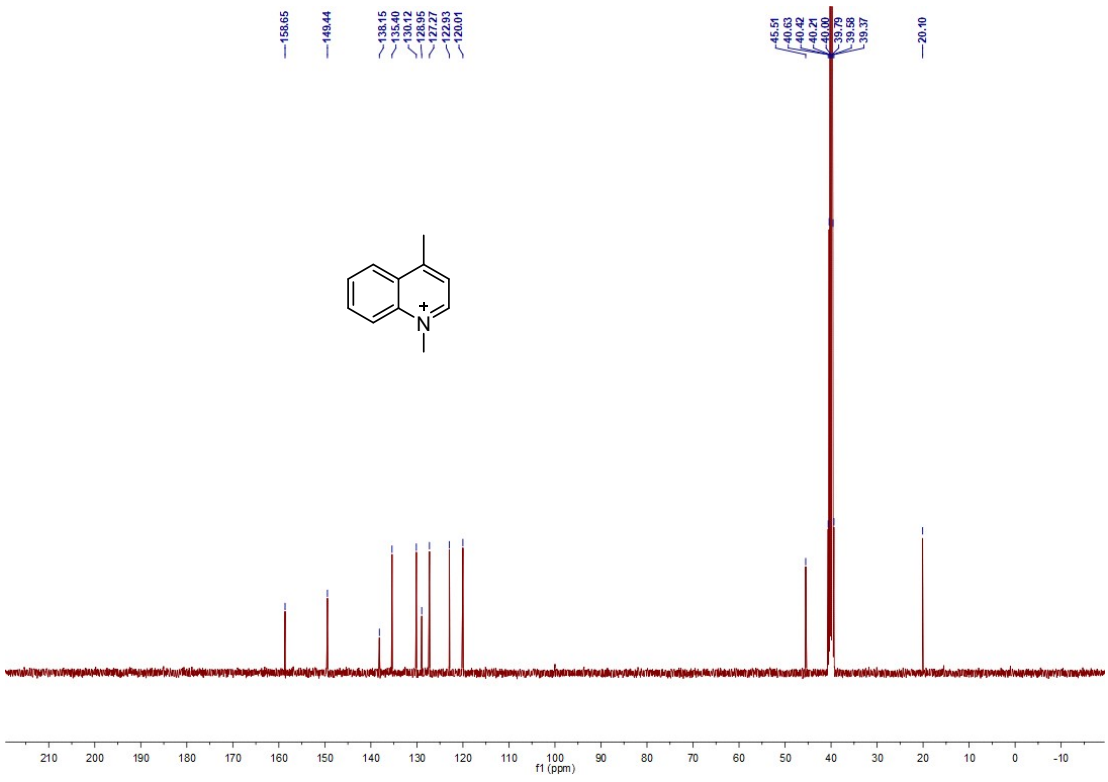

Fig. S41. [13]C NMR (100 MHz, 298 K, DMSO-d_6) spectrum for compound **4**.

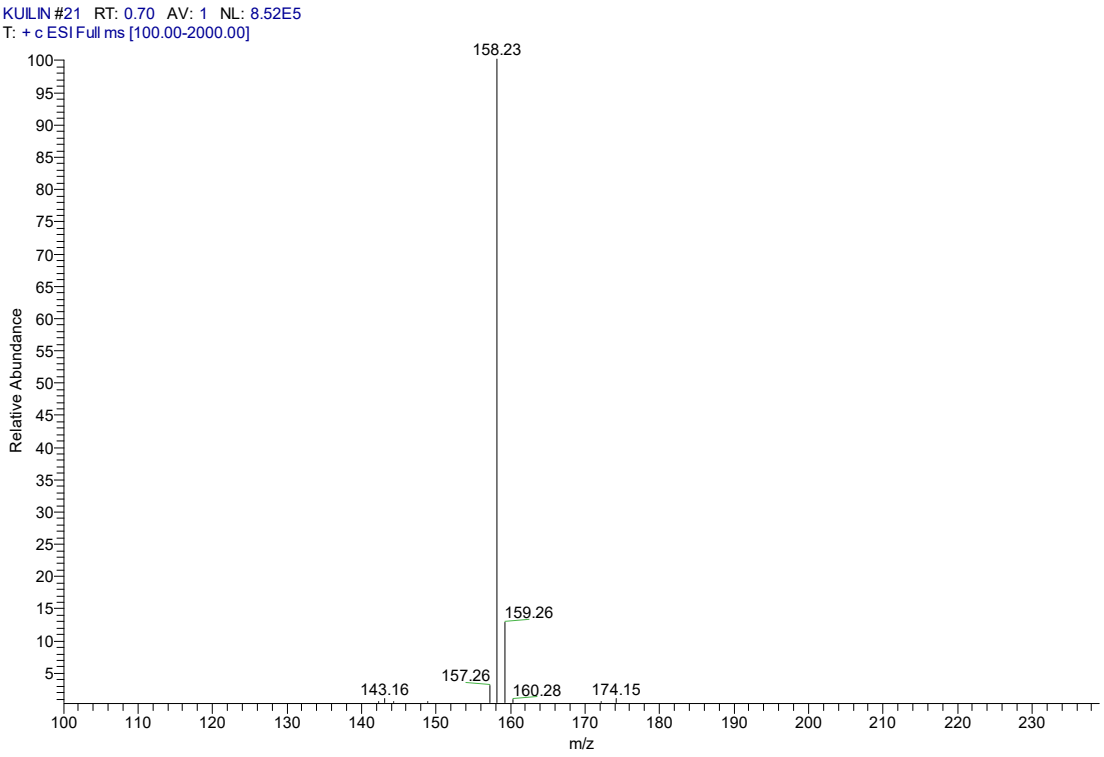

Fig. S42. MS-ESI spectrum for compound **4**.

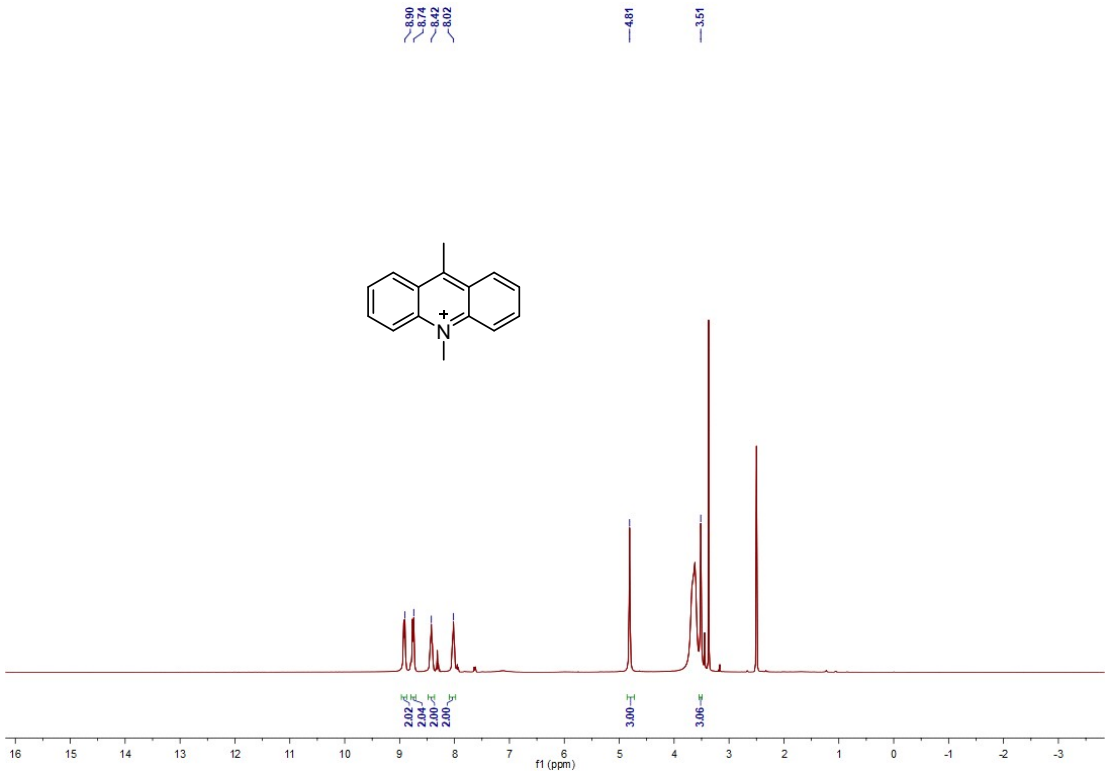

Fig. S43. ^{1}H NMR (400 MHz, 298 K, DMSO-d_6) spectrum for compound **5**.

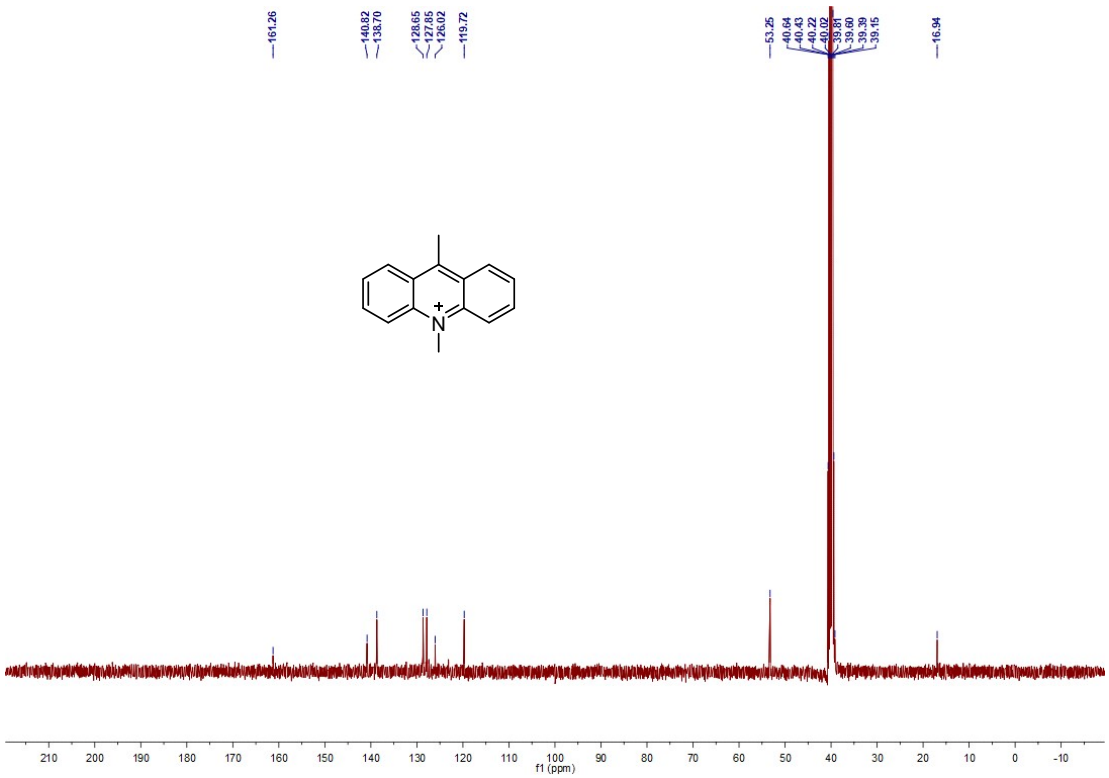

Fig. S44. ^{13}C NMR (100 MHz, 298 K, DMSO-d_6) spectrum for compound **5**.

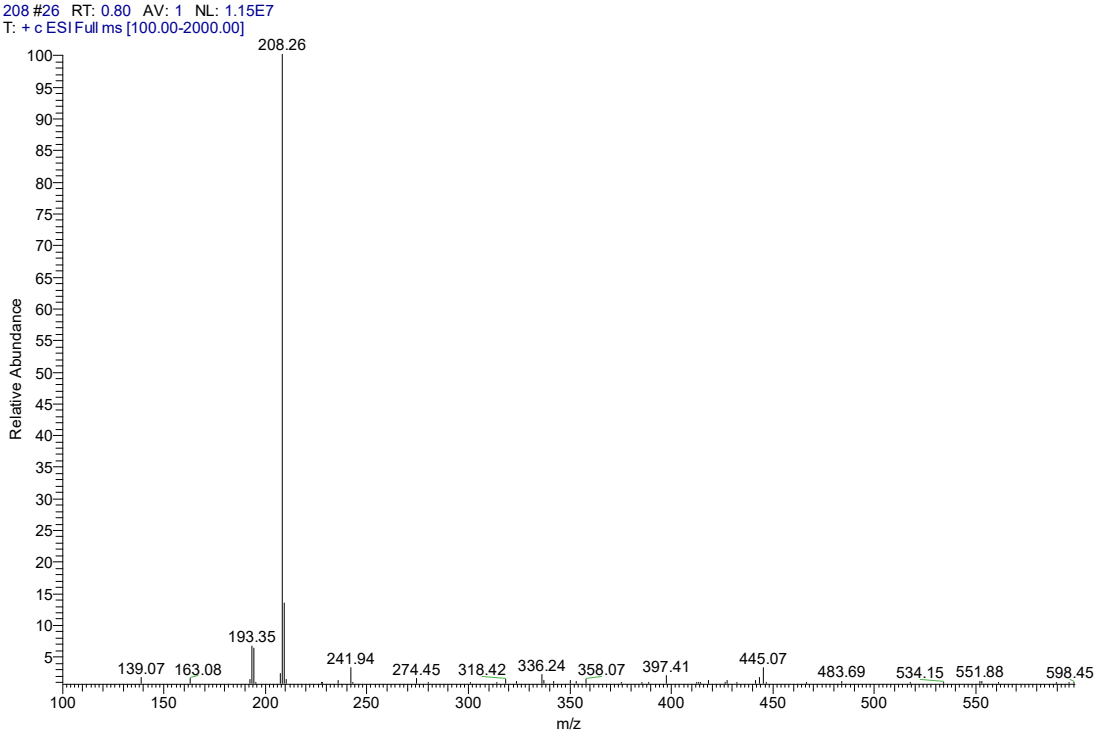

Fig. S45. MS-ESI spectrum for compound **5**.

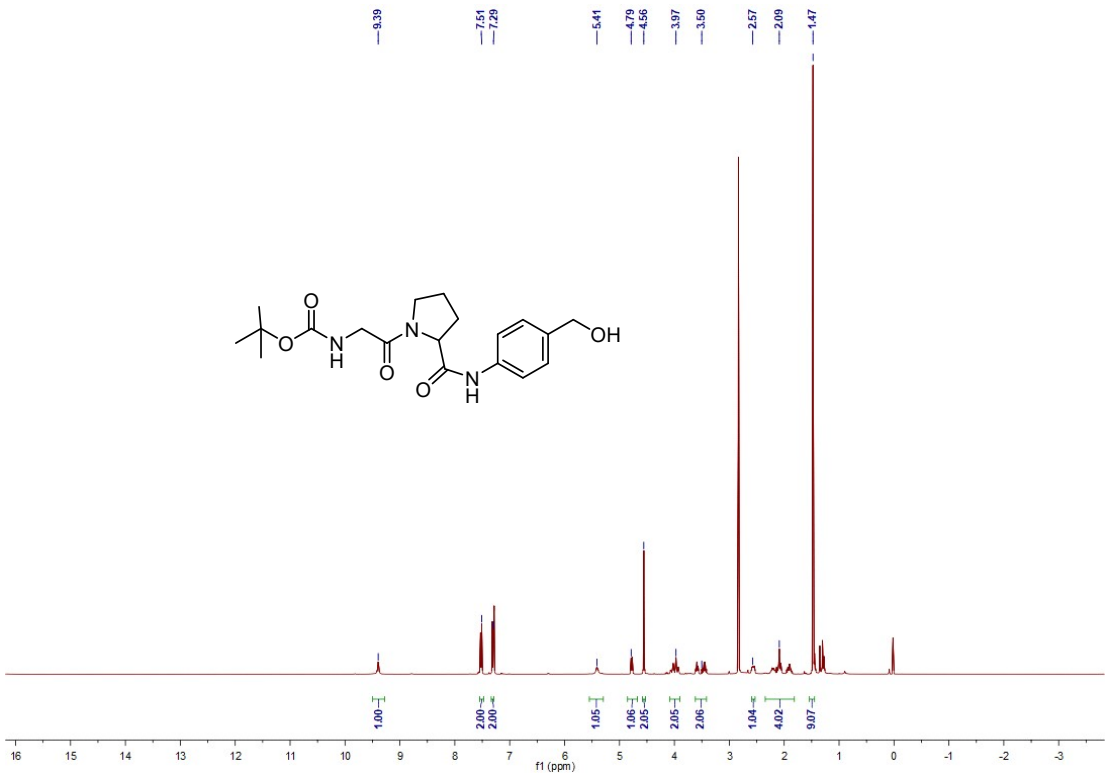

Fig. S46. ^{1}H NMR (400 MHz, 298 K, $CDCl_3$) spectrum for compound **6**.

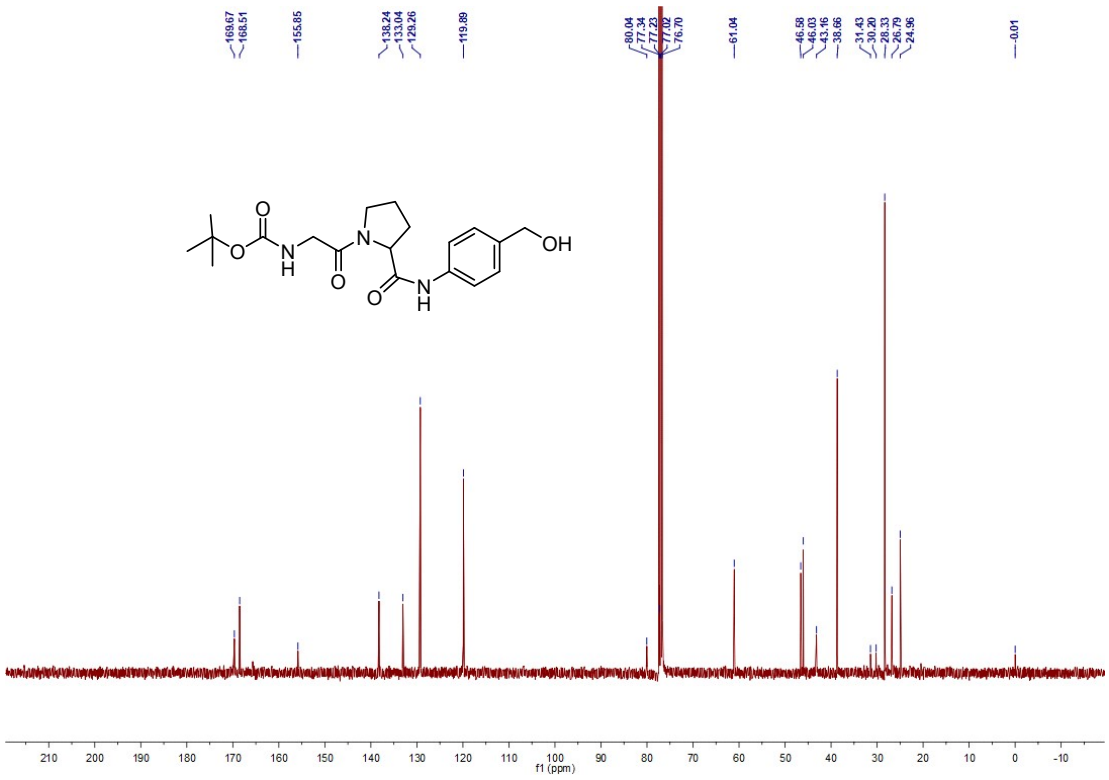

Fig. S47. ^{13}C NMR (100 MHz, 298 K, $CDCl_3$) spectrum for compound **6**.

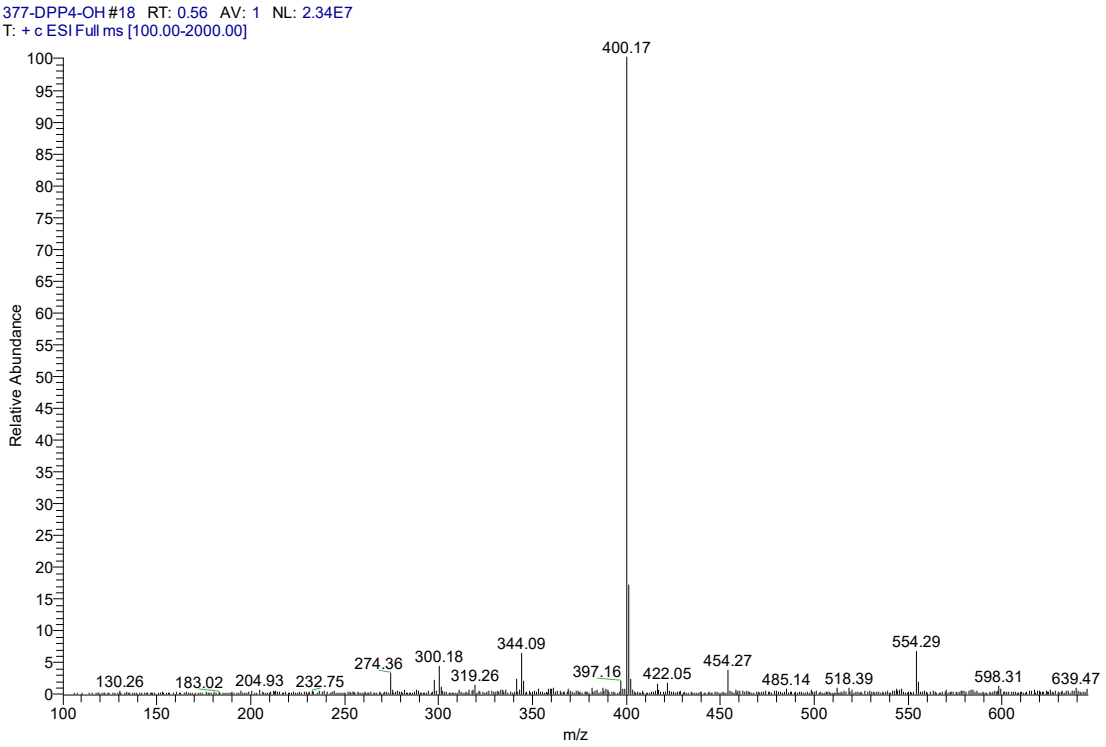

Fig. S48. MS-ESI spectrum for compound **6**.

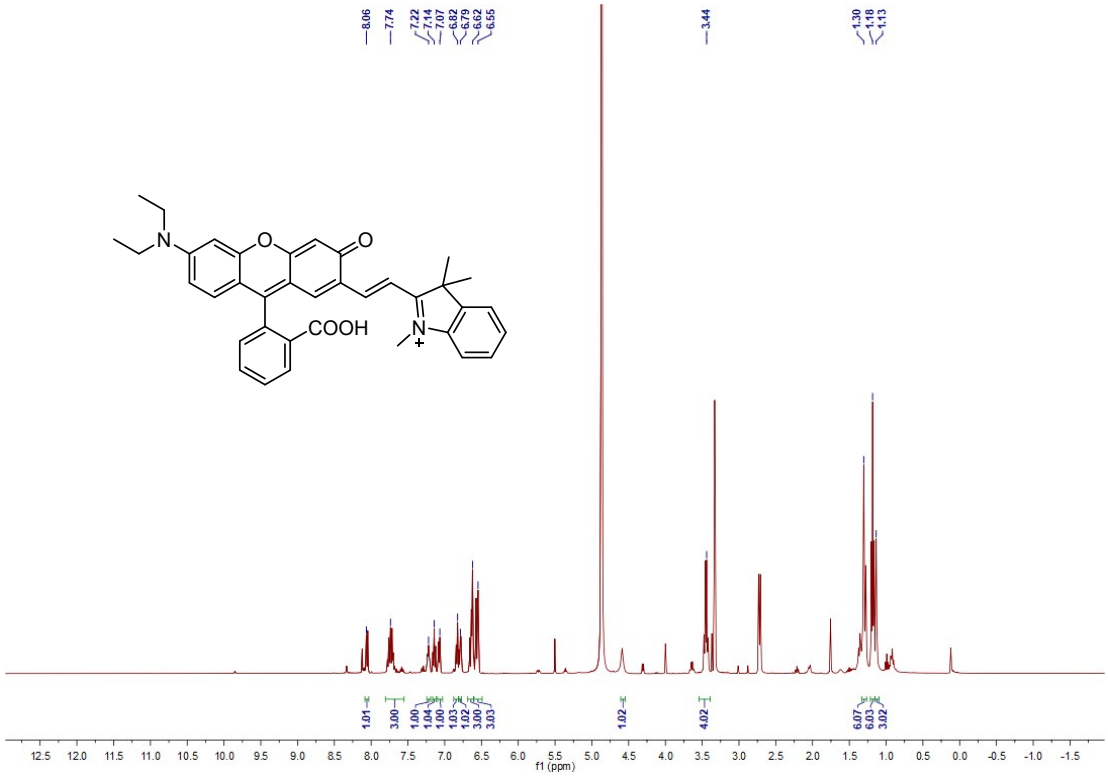

Fig. S49. ^{1}H NMR (400 MHz, 298 K, MeOD) spectrum for compound **RhoI**.

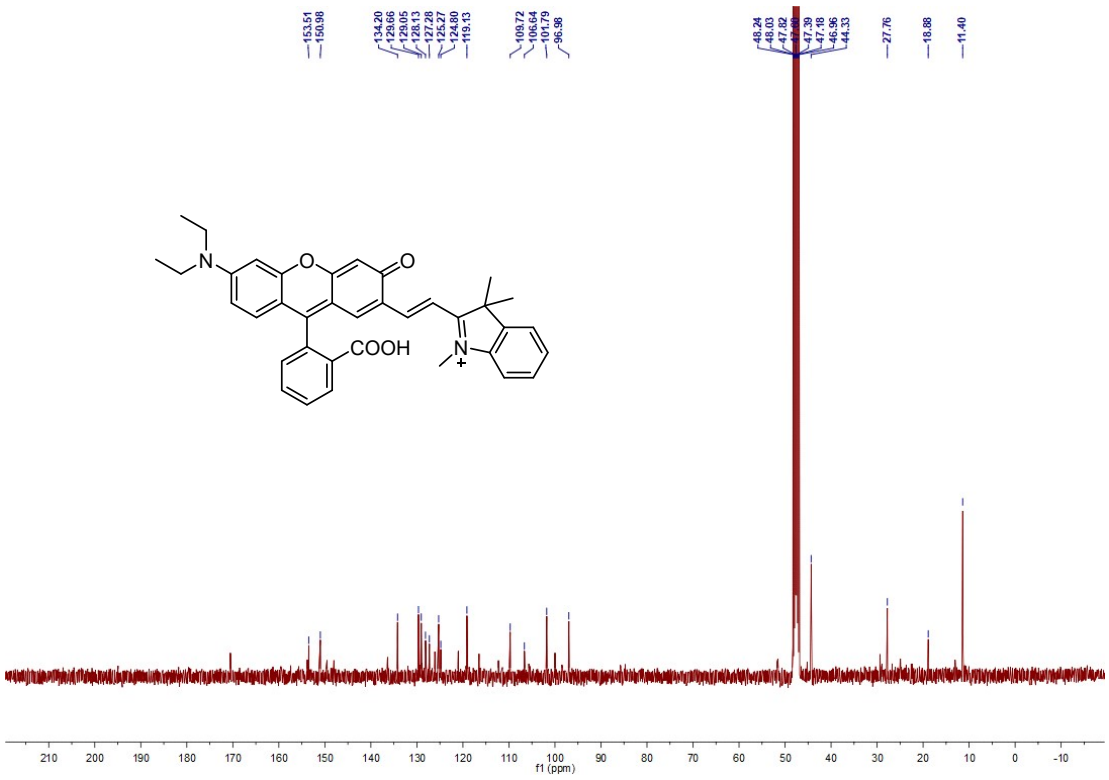

Fig. S50. ^{13}C NMR (100 MHz, 298 K, MeOD) spectrum for compound **RhoI**.

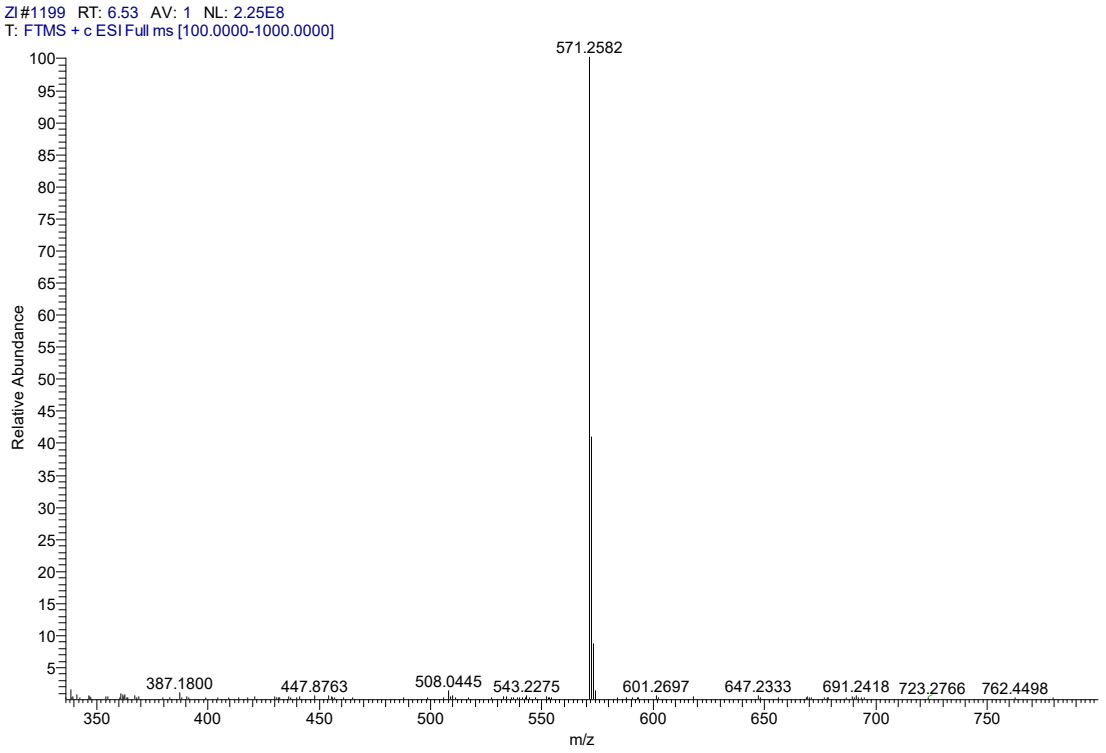

Fig. S51. HRMS spectrum for compound **RhoI**.

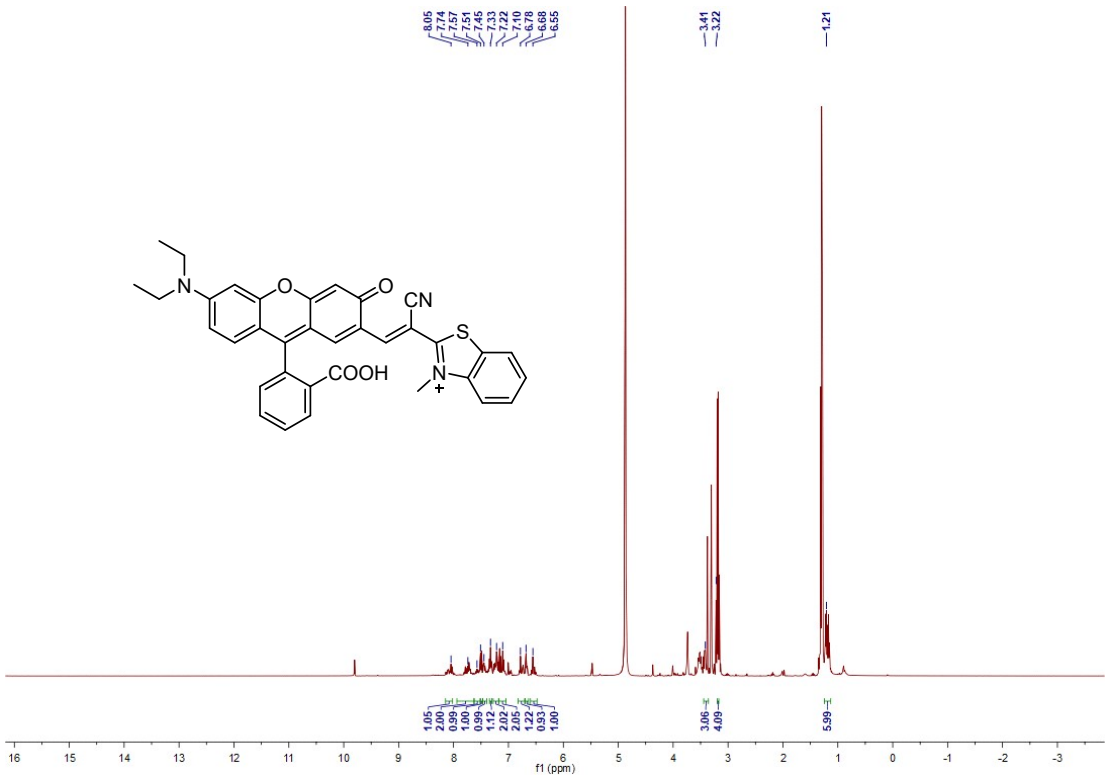

Fig. S52. [1]H NMR (400 MHz, 298 K, MeOD) spectrum for compound **RhoBTA**.

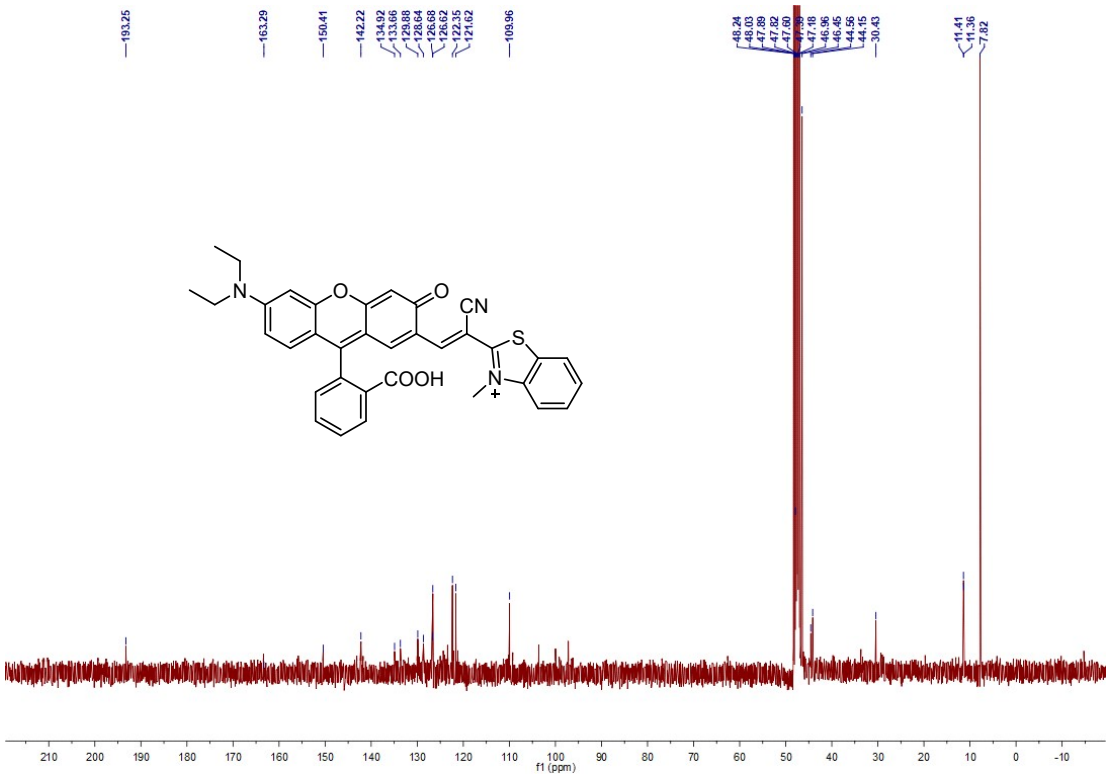

Fig. S53. [13]C NMR (100 MHz, 298 K, MeOD) spectrum for compound **RhoBTA**.

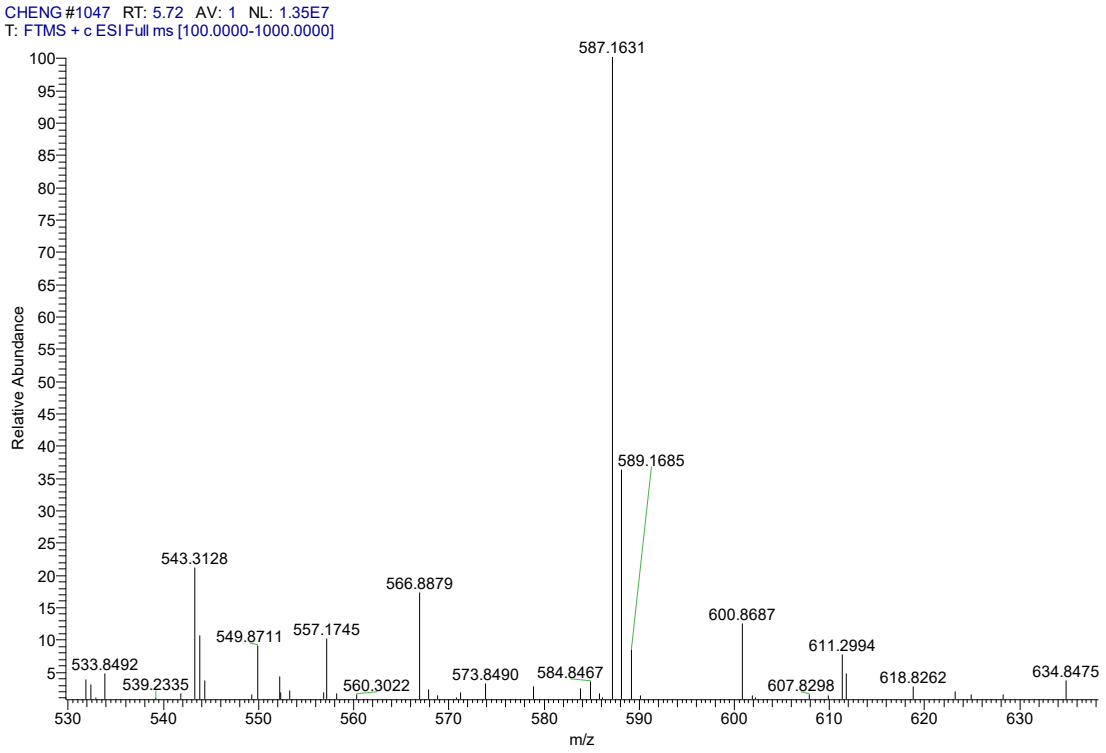

Fig. S54. HRMS spectrum for compound **RhoBTA**.

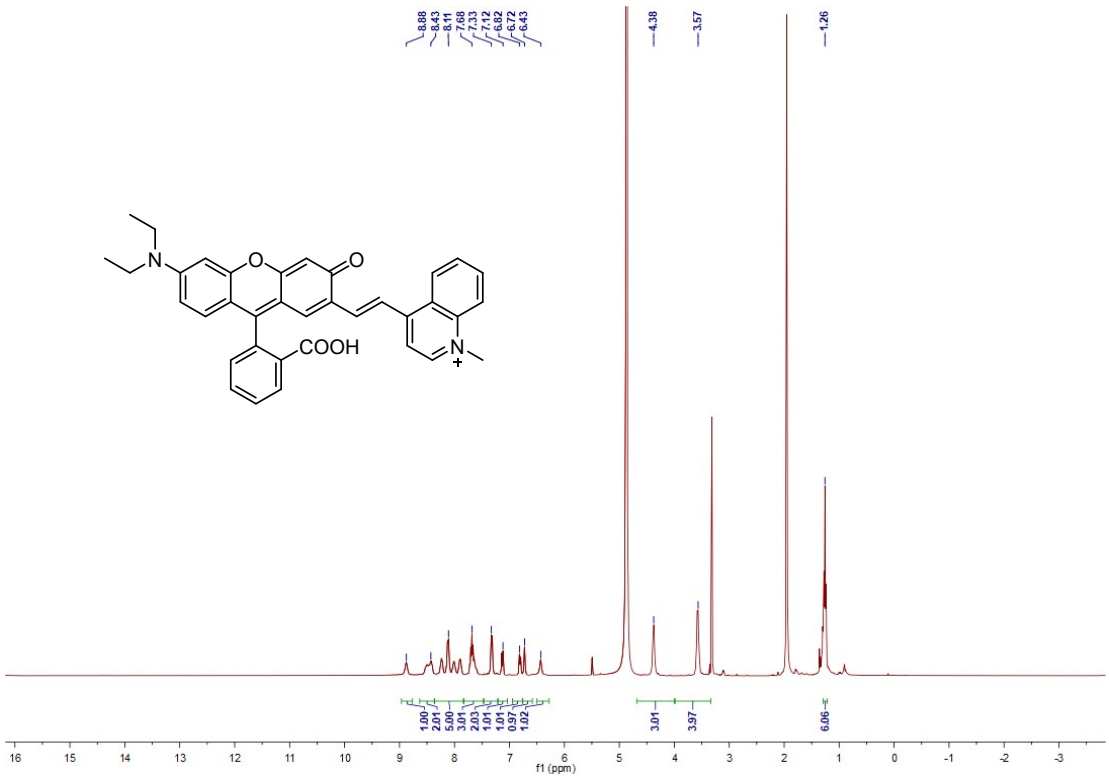

Fig. S55. ^{1}H NMR (400 MHz, 298 K, MeOD) spectrum for compound **RhoMQ**.

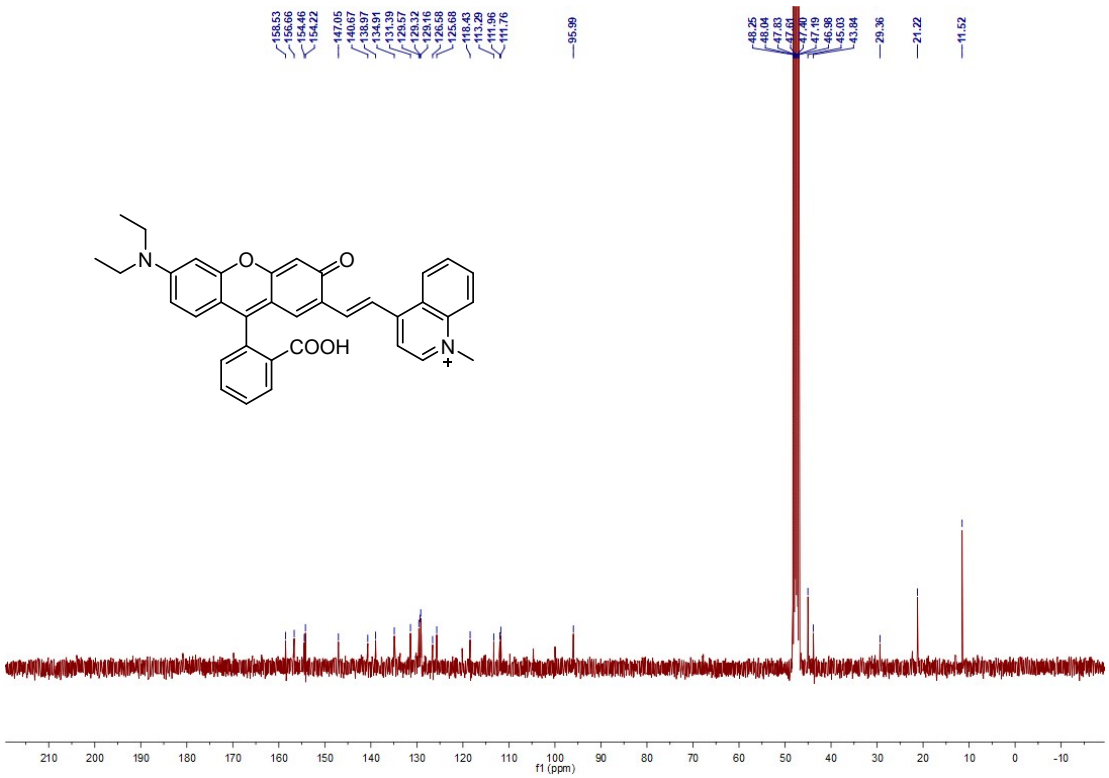

Fig. S56. ^{13}C NMR (100 MHz, 298 K, MeOD) spectrum for compound **RhoMQ**.

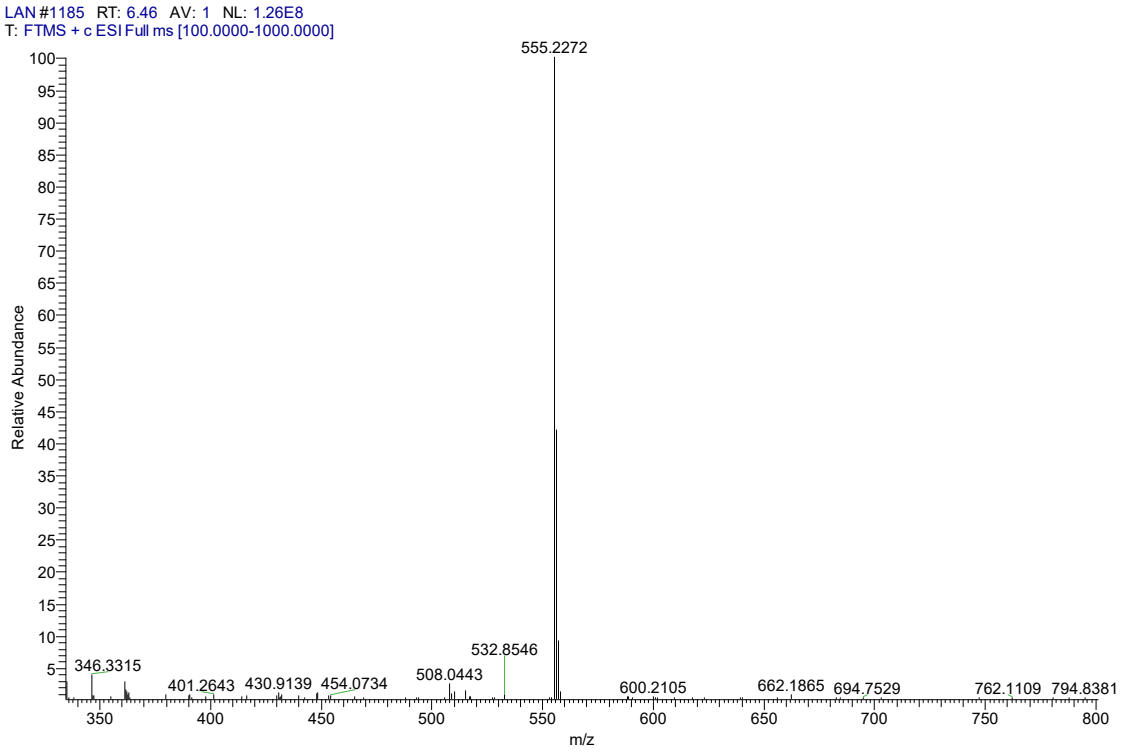

Fig. S57. HRMS spectrum for compound **RhoMQ**.

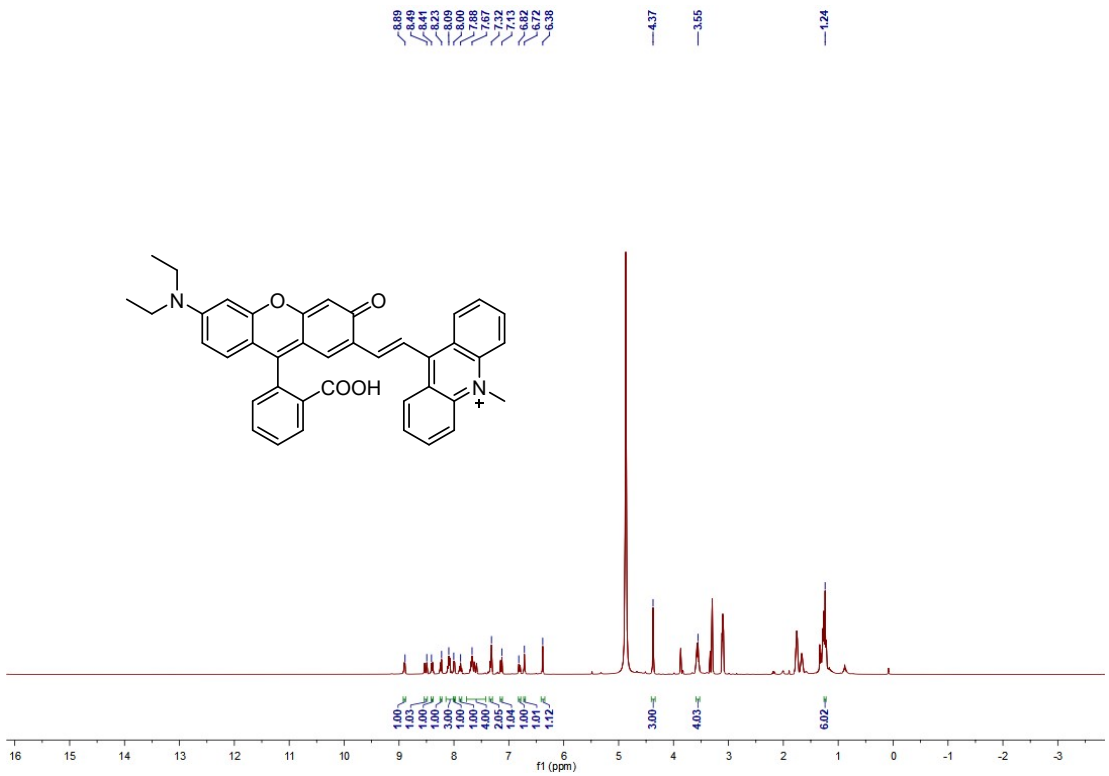

Fig. S58. [1]H NMR (400 MHz, 298 K, MeOD) spectrum for compound **RhoMA**.

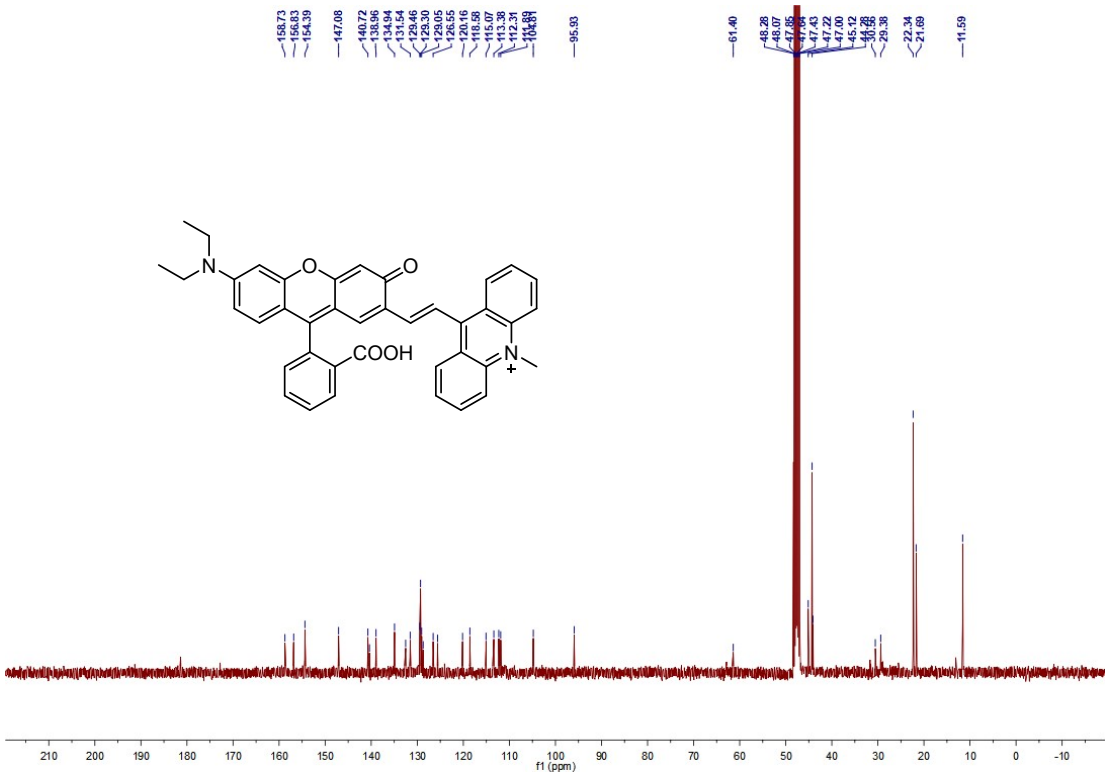

Fig. S59. [13]C NMR (100 MHz, 298 K, MeOD) spectrum for compound **RhoMA**.

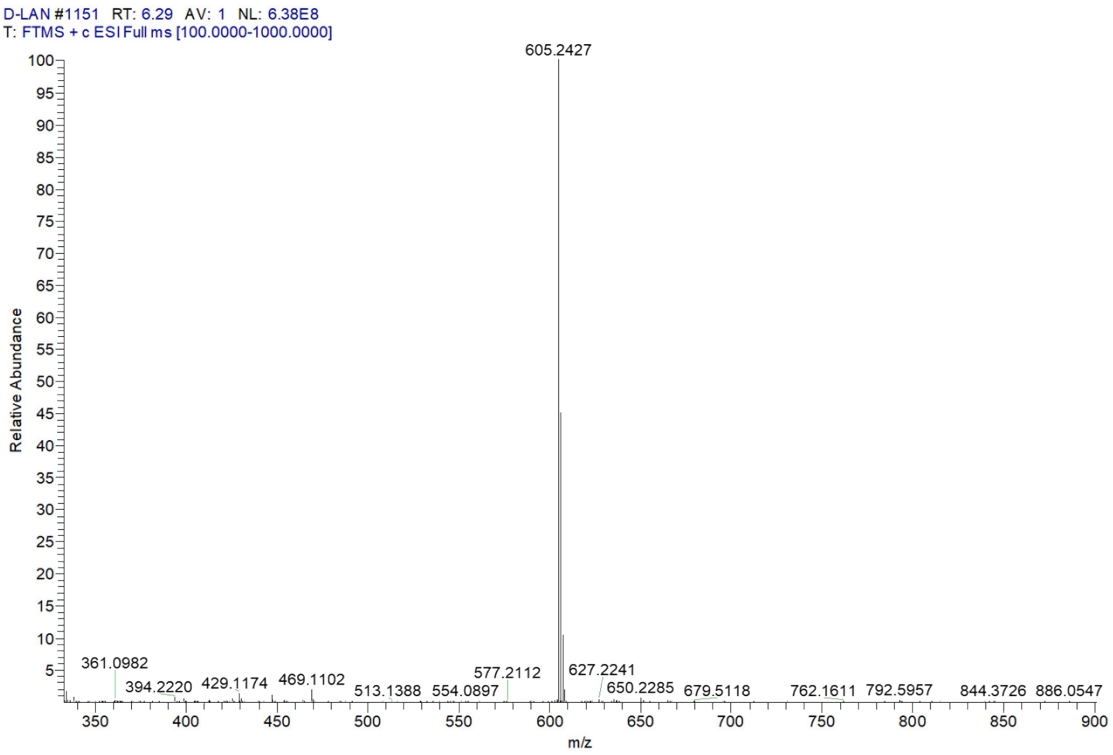

Fig. S60. HRMS spectrum for compound **RhoMA**.

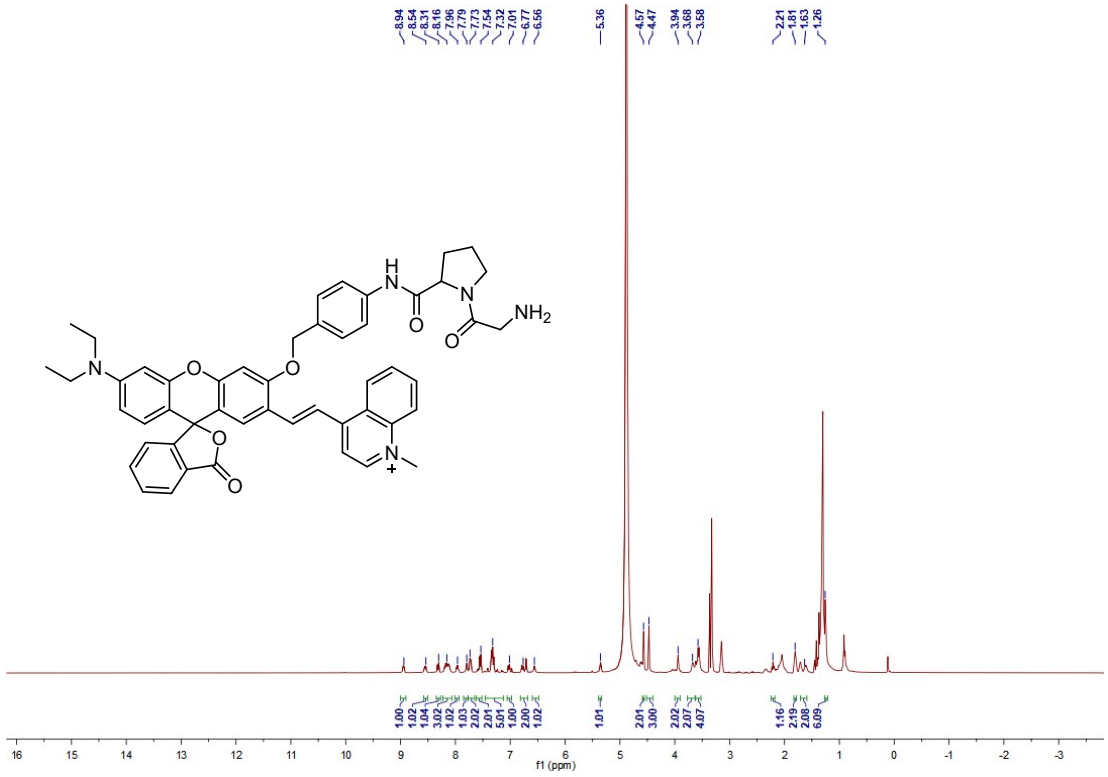

Fig. S61. ^{1}H NMR (400 MHz, 298 K, MeOD) spectrum for compound **RhoMQ-DPPIV**.

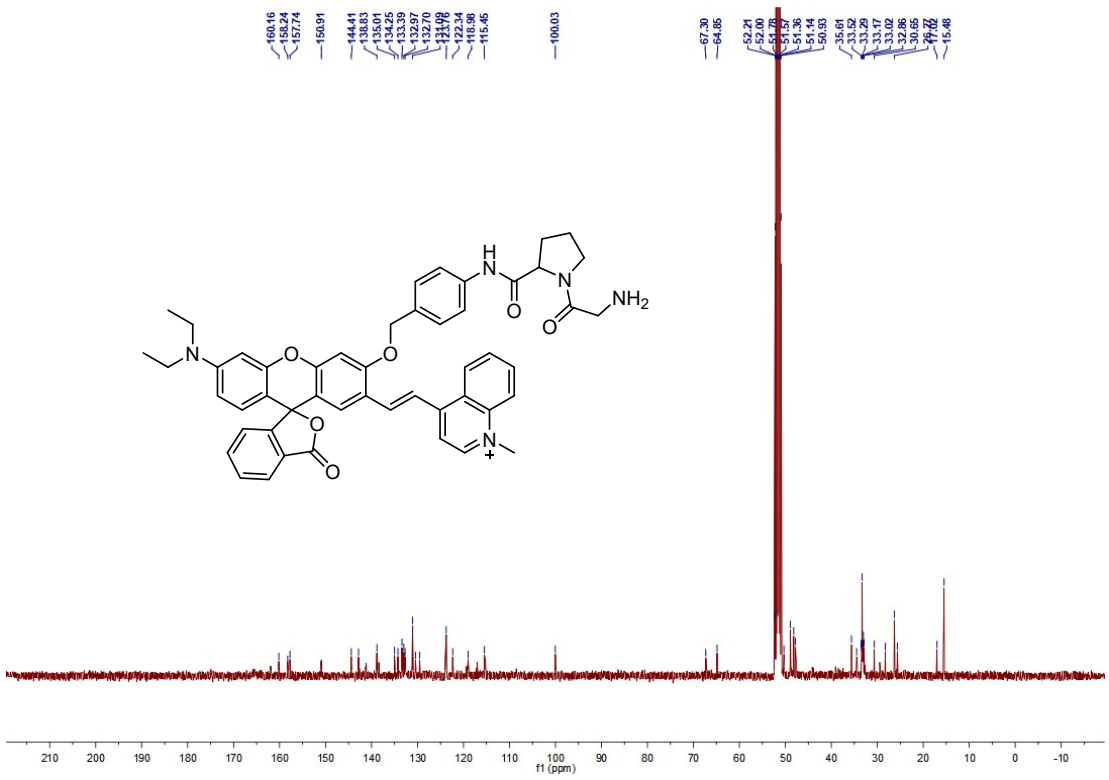

Figure S62. ^{13}C NMR (100 MHz, 298 K, MeOD) spectrum for compound **RhoMQ-DPPIV**.

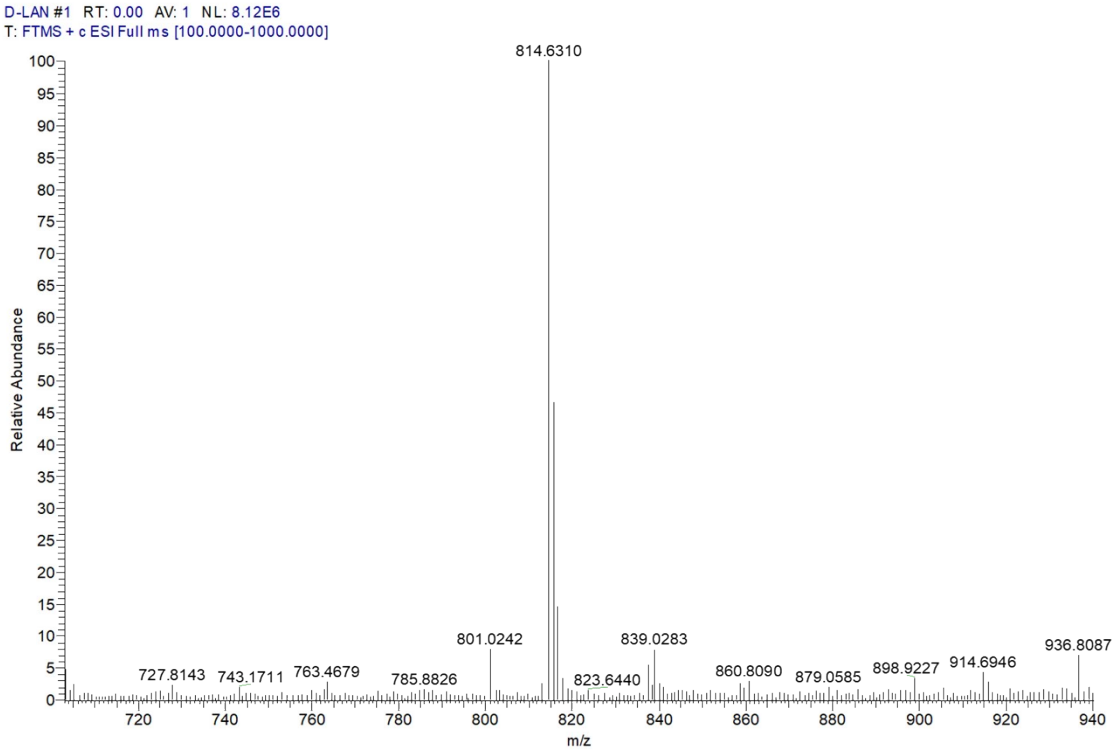

Fig. S63. HRMS spectrum for compound **RhoMQ-DPPIV**.

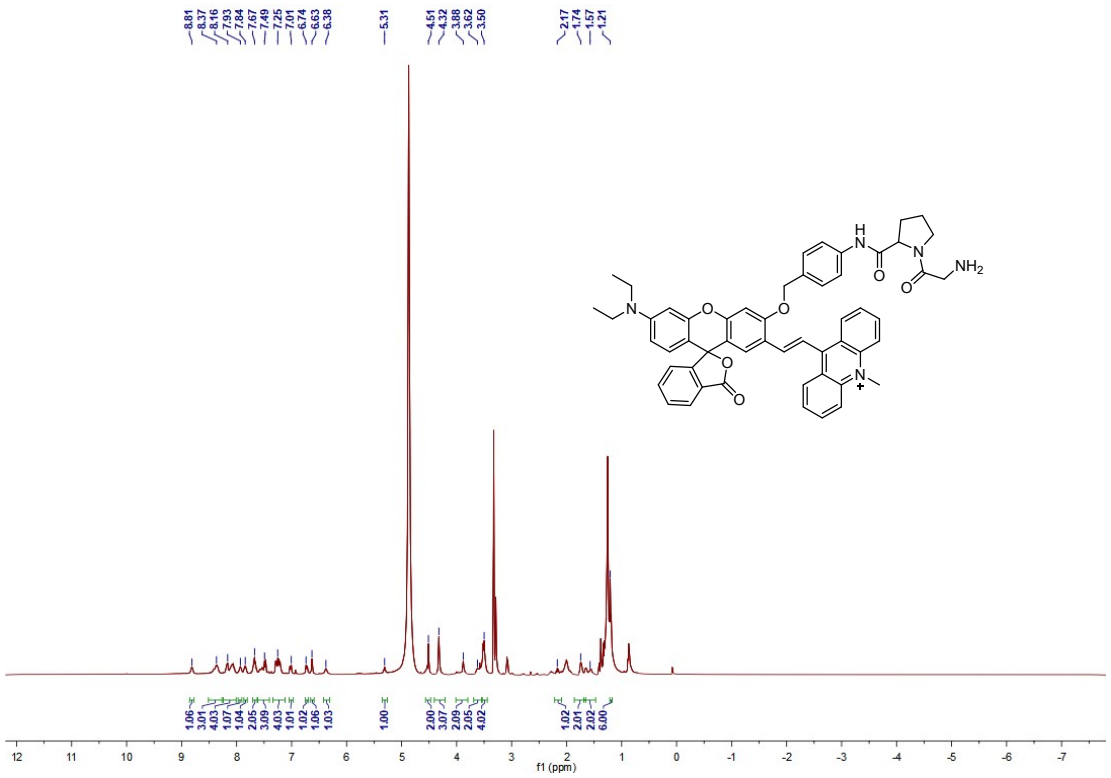

Fig. S64. ^{1}H NMR (400 MHz, 298 K, $CDCl_3$/MeOD) spectrum for compound **RhoMA-DPPIV**.

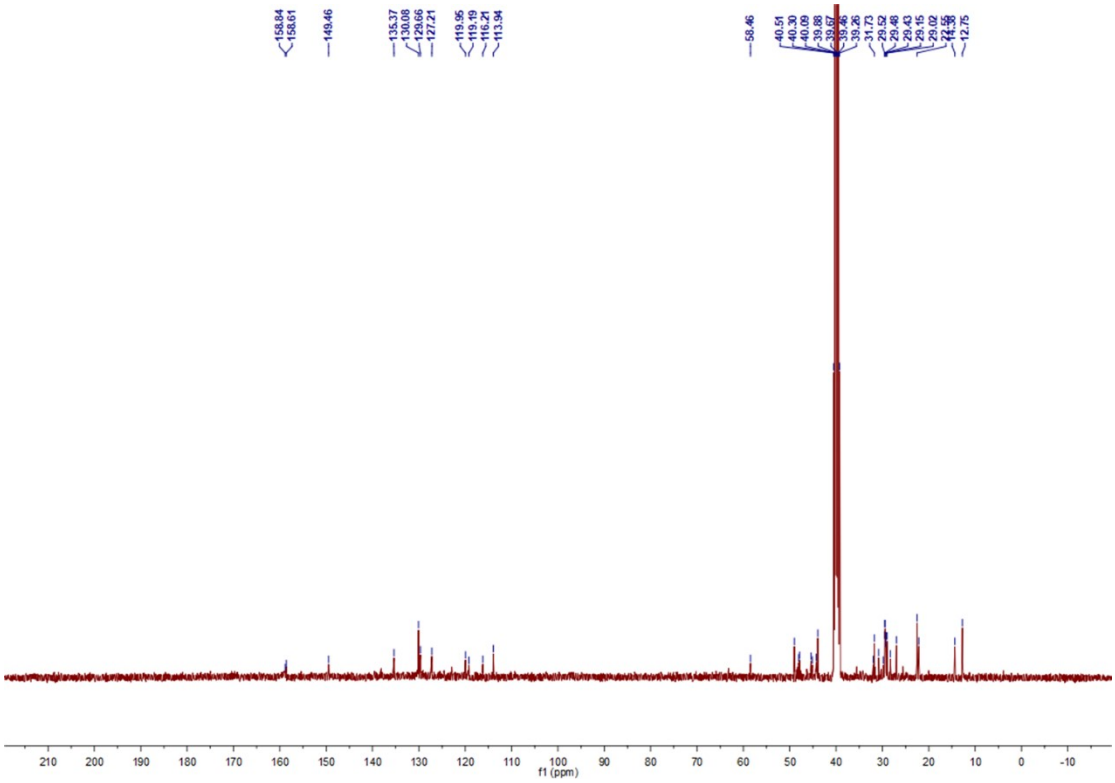

Fig. S65. ^{13}C NMR (100 MHz, 298 K, DMSO-d_6) spectrum for compound **RhoMA-DPPIV**.

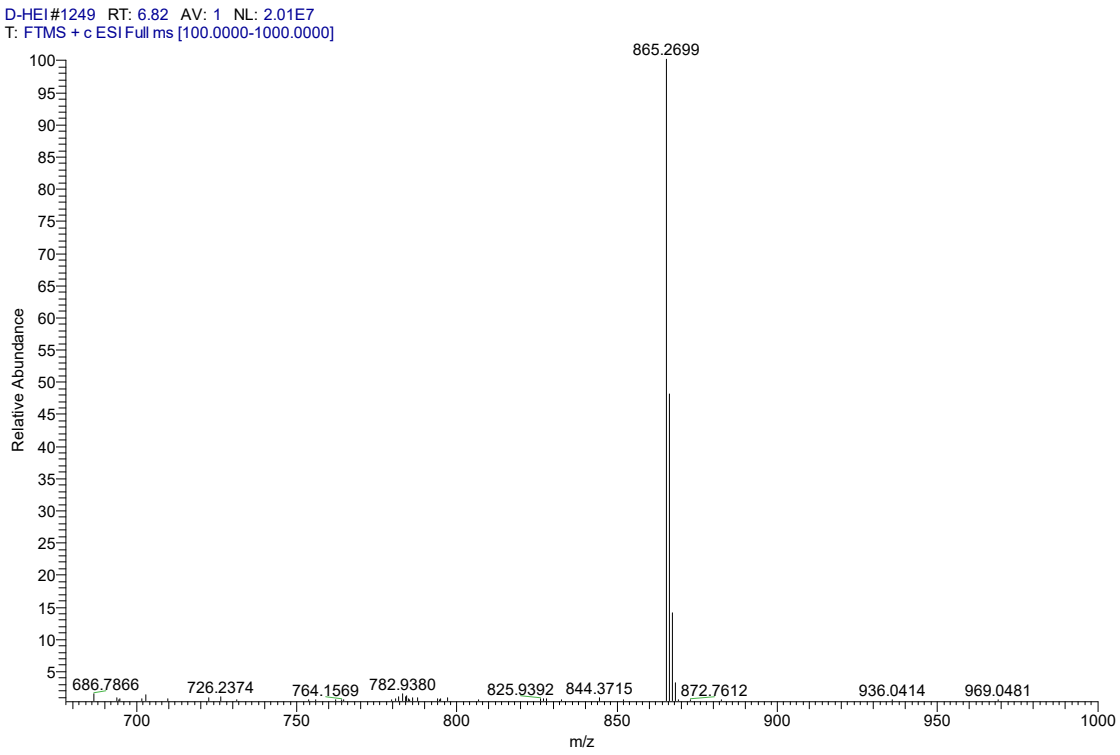

Fig. S66. HRMS spectrum for compound **RhoMA-DPPIV**.

5. References

1. R. B. Mujumdar, L. A. Ernst, S. R. Mujumdar, C. J. Lewis and A. S. Waggoner, *Bioconj. Chem.*, 1993, **4**, 105-111.